Catchment vegetation and erosion controls soil carbon cycling in south-eastern Australia during the last two Glacial-Interglacial cycles

Francke, A.[1-3*] , Dosseto, A. [1,2,4], Forbes, M. [4,5], Cadd, H.[4,6], Short, J.[7,8], Sherborne-Higgins, B.[2,4], Constantine, M. [6], Tyler, J.[3], Tibby, J.[7,8], Marx, S.[2,4], Dodson, J.[9], Mooney, S. [6], and Cohen, T.J.[2,4]

[1] Wollongong Isotope Geochronology Laboratory, School of Earth, Atmospheric and Life Sciences, University of Wollongong, Australia
[2] GeoQuEST Research Centre, School of Earth, Atmospheric and Life Sciences, University of Wollongong, Australia
[3] Department of Earth Sciences, University of Adelaide, Australia
[4] ARC Centre of Excellence for Biodiversity and Heritage, School of Earth, Atmospheric and Life Sciences, University of Wollongong, Australia
[5] KCB Australasia pyt ltd, Brisbane, Australia
[6] School of Biological Earth and Environmental Sciences, University of New South Wales, Australia
[7] Department of Geography, Environment and Population, University of Adelaide, Australia
[8] Sprigg Geobiology Centre, University of Adelaide, Australia
[9] Institute for Earth Environment, Chinese Academy of Science, Xi'an, Shaanxi, China

* corresponding author: alexander.francke@adelaide.edu.au

Abstract

The vegetation structure in vast semi-arid to temperate continental land masses, particularly in Australia, play a considerable role in global terrestrial carbon dioxide sequestration. However, whether soil-carbon is a net atmospheric carbon source or sink remains contentious, introducing large uncertainties on long-term storage of vegetation-sequestered carbon dioxide. We investigate the interplay between catchment erosion (quantified by means of uranium isotopes), vegetation (pollen), catchment carbon cycling, wetland response (diatoms), and lake carbon accumulation on glacial-interglacial timescales in south-eastern Australia during the last (133.5 ka to 107.6 ka) and current (17.8 cal ka BP to present day) glacial-interglacial cycle. The analyses are applied to the sediments of Lake Couridjah, located in the Sydney Basin, and are supported by uranium isotope and carbon contents of a ridge-crest soil pit from the vicinity of the lake.

Statistical analyses reveal robust phase-relationships between catchment erosion, vegetation composition, and carbon cycling during both glacial-interglacial periods. The data implies that vegetation structure, and not the amount of rainfall, had a more direct control on catchment erosion, and, thus, on SOC erosion in the catchment. Overall wetter and warmer (peak interglacial) conditions promoted the expansion of a canopy and mid-storey cover and reduced catchment erosion, while simultaneously increasing SOC storage, catchment and lake primary productivity, and lake carbon storage. The results may imply increased (reduced) terrestrial carbon dioxide sequestration in overall warmer and wetter (colder and drier) climates.

1. Introduction

Soil organic carbon (SOC) makes up to 80% of the terrestrial carbon pool (Doetterl et al., 2016). However, there is little information on the fate of SOC during soil erosion, introducing large uncertainties into national carbon flux estimates, Earth System Models (ESM), and General Circulation Models (GCM, Doetterl et al., 2016; Lugato et al., 2018; Francke et al., 2020a). Reanalysis of national greenhouse gas emissions in Australia, for example, has suggested that not considering cropland soil erosion overestimated the nation’s net carbon flux into the atmosphere by 40% (Chappell et al., 2015), explained by SOC lost by erosion and subsequently buried in sedimentary sinks rather than being re-oxidised (Chappell et al., 2015). This has led to an ongoing debate as to whether soil-carbon is a net atmospheric source or sink in the global carbon cycle (Chappell et al., 2015; Doetterl et al., 2016; Lugato et al., 2018), primarily related to gaps in our understanding of how lateral soil fluxes connect terrestrial and aquatic carbon cycling (Luo et al., 2016). These uncertainties become greater when constraining carbon fluxes on geological timescales, where “land use harmonization" (LUH) models integrated in GCMs or ESMs are based on landscape models such as HYDE (Klein Goldewijk et al., 2017) or KK10 (Kaplan et al., 2009). Direct vegetation modelling, which accounts for different pollen production and accumulation processes (e.g. LOVE, REVEALS, Sugita, 2007a; Sugita, 2007b; Trondman et al., 2015; Li et al., 2020) combined with quantitative estimates about catchment erosion, landscape change, and carbon cycling over time are still challenging to obtain (Francke et al., 2020a). Detailed multiproxy studies on erosion, vegetation, climate, and terrestrial-aquatic carbon cycling on geological timescales are one of the few approaches that can investigate these interactions simultaneously.

The arid, semi-arid, and temperate regions of the Southern Hemisphere are particularly important for understanding carbon fluxes, since wetter climates can significantly increase terrestrial biomass production in these regions, rapidly turning vast continental areas into globally significant carbon sinks (Haverd et al., 2013). This was demonstrated in Australia during the 2011 strong La-Niña event, when large areas of the continental interior experienced substantial 'greening', and a significant increase in global carbon uptake (Poulter et al., 2014; Haverd et al., 2016). Australia is also characterised by many ephemeral wetlands, and the wetting and drying of these systems has the potential to significantly affect carbon storage over various timescales.

Here we report an investigation of the catchment-wide dynamics of SOC and erosion at Lake Couridjah, part of the Thirlmere Lakes, located in temperate Australia, south-west of Sydney in the Sydney Basin (Fig. 1). Lake Couridjah provides an outstanding natural laboratory to study catchment-wide carbon cycling due to its small catchment (< 5 km^2), allowing catchment changes to be readily transmitted to lake sediments. In addition, its temperate climate is characteristic of wide parts of south-eastern (SE) Australia, its uniform sandstone lithology is widespread across Australia, and its location within a World Heritage Listed National Park that has preserved intact its dry sclerophyll native vegetation makes Lake Couridjah an excellent study site. Furthermore, Lake Couridjah's lacustrine sediments span at least the last and current glacial-interglacial cycle (Forbes et al., 2021), allowing examination of the interplay between vegetation, erosion, SOC mobility, and wetland response under various climatic conditions.

We used a multi-proxy approach, studying soil and sedimentary total organic carbon, as well as palaeoecological data (pollen, charcoal, diatoms) to consider catchment-wide SOC cycling. We overcome current analytical limitations to quantify catchment-wide erosion in fine-grained depositional archives by using the uranium isotope compositions (^{234}U and ^{238}U) of fine-grained detrital matter to infer palaeo-sediment residence times. This is defined as the time elapsed between comminution of bedrock in the weathering horizon and the final deposition in the sedimentary sink (Fig. 2). The conceptual model introduced by DePaolo et al. (2006) is based on α-recoil induced depletion of the intermediate radioactive nuclide ^{234}Th from fine-grained detritus in the weathering profile, during transportation, temporary storage, and after final deposition (reviewed in Dosseto and Schaller, 2016; Francke et al., 2020a). Recent research has further substantiated the approach via detailed assessments of uranium mobility before and after final deposition (Martin et al., 2019; Francke et al., 2020b), and by comprehensive statistical analyses of lithologic, weathering, climatic, and morphologic controls on ($^{234}U/^{238}U$) activity ratios in modern stream sediments (Thollon et al., 2020).

2. Material and Methods

2.1 Regional Setting

Lake Couridjah is part of the Thirlmere Lake system (34°13'S; 150°13'E), which consists of five lakes (total basin area of 4.85 km^2) located approximately 100 km south-west of Sydney (Australia) at 300 m above sea level (Fig. 1). The Thirlmere Lakes are located within an abandoned, Cenozoic meandering river valley with a distinctive U-shaped arrangement (Timms, 1992).

The morphology of the Thirlmere Lakes catchment is characterised by steep Hawkesbury Sandstone scarps (20 – 30 m in height) grading to plateau surfaces ~ 50 to 75 m above the lake floor. Small Pleistocene alluvial fans separate the five lakes and form gently inclined slopes to the valley floor. Readily erodible shales of the Wianamatta Group, capping the Hawkesbury Sandstone, have limited exposure in the Thirlmere catchment today (Forbes et al., 2021).

The present day vegetation at Thirlmere has previously been described by Black et al. (2006), Rose and Martin (2007) and Forbes et al. (2021). A detailed survey of the contemporary vegetation in the vicinity of Lake Couridjah shows the catchment is presently dominated by an open sclerophyll forest (Forbes et al., 2021, Fig. 1 and Supplementary information).

Average summer and winter temperatures at Thirlmere are 29°C and 10°C, respectively (Bureau of Meteorology, 2021). Annual evaporation (1400 to 1600 mm.yr^{-1}) exceeds annual precipitation (800 mm, Bureau of Meteorology, 2021). Precipitation is distributed evenly across seasons, with summer precipitation associated with north-easterly weather systems (tropical derived East Coast Lows and easterly troughs, and onshore anticyclonic ridges) and winter precipitation with north-westerly moving air-masses. This seasonal pattern results from the system's location at the latitudinal transition zone between the mid-latitude westerly and tropical-influenced synoptic-weather systems. Variations in annual and decadal rainfall amounts in SE Australia are linked to interactions between El-Niño Southern Oscillation (ENSO), the Pacific Decadal Oscillation (PDO) variability, the Southern Annual Mode (SAM), and the Indian Ocean Dipole (IOD), and are mainly expressed by variations in winter rainfall (van Dijk et al., 2013). The Thirlmere Lakes are presently characterised as ephemeral, however, water depths up to 5 m were reported during the 1950 - 1960s (Horsfall et al., 1988). The lake levels closely follow reconstructed water levels of other lakes in SE Australia during the last century (Short et al., 2020), implying the Thirlmere Lakes are highly sensitive to regional climate forcing.

2.2 Palaeolimnology and chronostratigraphy

A comprehensive, multidisciplinary palaeolimnological and chronostratigraphic study has previously been carried out on a 6.8 m long sediment core (LC2) from the central part of Lake Couridjah. Sedimentary (grain size, mineralogy), geochemical (major inorganic and organic element geochemistry, carbon and nitrogen stable isotopes, ^{13}C-Nuclear Magnetic Resonance), palaeoecological (pollen, diatoms, charcoal, chironomids) and chronostratigraphic (radiocarbon [^{14}C] and optically stimulated luminescence [OSL]) data are presented in Forbes et al. (2021). In summary, chronostratigraphic (13 ^{14}C and nine OSL) and sedimentary data indicated the lower part of LC2 covers the time intervals between ~133.5 ka and ~107.6 ka (6.8 m to 3.2 m dated by means of single grain optically stimulated luminescence [OSL] reported as kilo annum, ka), and the upper part the time interval between ~17.8 cal ka BP and present day (3.2 m to 0 m dated by means of AMS radiocarbon dating and calibrated using the SHCal20, and reported as calibrated years before present, cal. ka BP, Fig. S1). A major hiatus was identified at 3.2 m sediment depth, between these two intervals (Forbes et al., 2021). Sediments attributed to warmer and wetter intervals are characterised by high sedimentary organic matter (OM) contents and the sediments are classified as peat (for the Holocene) and organic silty clay (between 130 ka and 115 ka, broadly corresponding to marine isotope stage (MIS) 5e, Fig. S1). Interstadial (115 ka to 107.6 ka, broadly corresponding to MIS5d) and glacial (133.5 ka to 130 ka broadly corresponding to the penultimate glacial, and 17.8 cal ka BP to 11.6 cal ka BP corresponding to the Late Glacial) sediments show lower OM contents and were characterized as organic silty clay, silty clay, and sandy clay (Forbes et al., 2021).

2.3 Methods

X-ray fluorescence (XRF) core scanning, organic carbon content, diatom, charcoal, and pollen data and their methods have been reported in Forbes et al. (2021). Previously unpublished data presented in this study comprise uranium isotope analyses on LC2 and bedrock samples (outcrop and drill hole samples), as well as uranium isotopes, organic carbon content, and major element concentrations (titanium and potassium) on a 50 cm soil pit (Werri Berri Ridge Crest 1 - WBRC1) located on the ridge crest of neighbouring Lake Werri Berri. Six 5 cm thick samples were taken consecutively from the upper 35 cm, with a final sample taken at 50 cm (the soil-saprolite interface). Major element concentrations were analysed using standard techniques (see Supplement for more details).

Uranium isotope analysis of six soil, 31 sediment (1 cm thick, core LC2), and bedrock (four outcrop and one drill core samples) was carried out at the Wollongong Isotope Geochronology Laboratory, University of Wollongong. All soil and sediment samples were sieved to 63 µm, and the fine fraction was used for further analyses. Sonication-supported sequential leaching to remove non-detrital matter from the bulk soil and sediment sample and hydrofluoric-nitric and aqua regia sample dissolution followed the method described in Francke et al. (2018). Bedrock samples were crushed and powdered and the same procedure for sample dissolution as described for the soil and sediment samples was applied. Uranium was separated from the sample matrix using the automated chromatography system prepFAST-MC™ (Elemental Scientific) equipped with a company (Elemental Scientific) provided column ThU1 – 0500. The samples were refluxed in 7M HNO_3 prior to chromatography, and Th and U were eluted in IQ 6M HCl and 18.2 MΩ H_2O. A ThermoFisher (Bremen, Germany) Neptune multi-collector inductively coupled plasma mass spectrometer (MC ICP-MS) was used for uranium isotope analyses. Details on mass spectrometry analysis and on analytical accuracy and precisions are reported in the Supplement. A subset of chemically treated (sequential leaching applied) lake core samples were analysed for surface area and roughness on a Quantachrome Autosorb iQ (Table S3) using the method described in Francke et al. (2018) and in the Supplement.

2.4 Calculations

To calculate palaeo-sediment residence times, we used equations developed by Martin et al. (2019) and Francke et al. (2020b) to account for preferential leaching of ^{234}U before and after deposition separately. Preferential leaching can promote lower ($^{234}U/^{238}U$) activity ratios in detrital grains that is not related to recoil-loss of ^{234}Th. Different scenarios for pre- and post-depositional preferential leaching of ^{234}U and different scenarios for (reduced) loss of ^{234}Th by recoil after final deposition were tested (see Supplement). Palaeo-sediment residences times were calculated for LC2 using Monte Carlo simulations (10,000 simulations) to account for uncertainties in our input parameters using an R64 script (available upon request to the authors).

Partial Least Square Regression (PLSR) analysis was performed on previously published pollen relative abundance data (as predictor variables) and palaeo-sediment residence times (as response variables) to consider relationships between vegetation change and catchment erosion. Aquatic and semi-aquatic pollen taxa (such as Cyperaceae) were excluded from the total pollen sum and relative abundances were re-calculated for terrestrial taxa (Forbes et al., 2021, supplement). Chenopodiaceae pollen was excluded from the terrestrial pollen sum as it occurred at very low percentages, likely indicating it is derived by windblown transportation from outside the catchment (Dodson, 1983; Williams et al., 2006). Re-calculated relative abundances of Myrtaceae + Casuarinaceae, *Acacia* (genus), Asteraceae (Asteroideae or Tubuliflorae), and Poaceae and palaeo-sediment residence times were normalized (mean = 0, standard deviation = 1) prior to PLSR analyses. PLSR analyses was undertaken for current and last glacial-interglacial sediments separately.

3. Results

3.1 Modern catchment data

Uranium isotopes of samples from unweathered Hawkesbury Sandstone from a core penetrating ~21 m into the bedrock reveal ($^{234}U/^{238}U$) activity ratios above 'secular equilibrium' (($^{234}U/^{238}U$) activity ratios = 1). Bedrock collected from outcrops in the Thirlmere catchment show significant depletion in ^{234}U (Fig. 3). Uranium isotope analyses of the 50 cm deep soil pit WBRC1 located on the ridge crest of neighbouring Lake Werri Berri yielded ($^{234}U/^{238}U$) activity ratios between 0.856 and 0.892, thus showing expected recoil-induced depletion of ^{234}U in fine-grained (<63 µm) detrital matter. The activity ratios increased with greater soil depth (Fig. 3).

K/Ti ratios of bulk-detrital soil samples between 0 cm and 35 cm depth in WBRC1 are low and steady (K/Ti = 0.4 to 0.5, Fig. 3). High ratios occur in the sample taken at 50 cm depth and in the underlying saprolite (K/Ti = 2.2). SOC, as inferred from WBRC1 soil-TOC, is between ~1 and 3.9 %, with values >1.5% only found in the upper 20 cm. The OM-rich topsoil layer overlayed a thick sandy horizon with poor vertical soil stratification, classifying WBRC1 as skeletal soil.

3.2 The last and current glacial-interglacial cycle

Monte-Carlo modelled palaeo-sediment residence times (i.e. time elapsed between comminution and final deposition reported in kyr, Fig. 2) ranged from 15 to 70 kyrs in sediments deposited between 133 ka to 130 ka (broadly equivalent to MIS 6), between 115 ka and 107.6 ka (broadly equivalent to MIS5d), and between 17.8 cal ka BP and 11.6 cal ka BP (Late Glacial), respectively. Longer residence times, between 70 kyrs and 124 kyrs, were evident between depositional ages of 130 ka and 115 ka (broadly equivalent to MIS5e), between 17.8 cal ka BP and 16 cal ka BP, and during the Holocene (11.6 ka to present day).

Terrestrial pollen taxa abundance indicate Lake Couridjah's catchment vegetation was composed of sclerophyll trees and shrubs (Myrtaceae + Casuarinaceae between 44% and 86%) during both the last (133.5 ka to 107.6 ka) and current (17.8 cal ka BP to present day) glacial-interglacial (Fig. 4). The pollen of *Acacia* (0.6% to 3.5%) genus occurs at low abundance during both climate cycles. Herb and grassland vegetation cover, comprising of Asteraceae (Asteroideae or Tubuliflorae, 1% to 48%) and Poaceae (2.5% to 22.5%) contributed substantially to the vegetation composition in the Thirlmere catchment during both glacial-interglacial cycles. Broadly, higher proportions of arboreal taxa (Myrtaceae + Casuarinaceae and-or *Acacia*) and lower proportions of understorey taxa (Asteraceae and Poaceae) occurred during warmer and wetter intervals (130 ka and 115 ka and during Holocene, Fig. 4). Peaks in macroscopic charcoal area ($mm^2/cm^3/yr$) between 130 ka and 115 ka and during Last Glacial corresponded to declines in Myrtaceae + Casuarinaceae and-or *Acacia* (Fig. 4). Stable Polycyclic Aromatic Carbon (SPAC) abundance was higher between 130 ka and 115 ka, 106 ka and 103 ka, and during the Holocene (Fig. 4).

PLSR analyses of terrestrial pollen taxa (Myrtaceae + Casuarinaceae, *Acacia,* Asteraceae, Poaceae) and palaeo-sediment residence times were preformed separately for the last and current glacial-interglacial cycle (Fig. 5). The statistical analysis reveals strong positive loading on predictor axis 1 for Myrtaceae + Casuarinaceae and *Acacia* during the last glacial-interglacial (Fig. 5). Only Myrtaceae + Casuarinaceae shows strong positive loadings on predictor axis 1 for the current glacial-interglacial (between 17.8 cal yr BP and present). Asteraceae and Poaceae have strong negative loadings on PLSR predictor axis 1 in the last glacial-interglacial (133 ka to 107 ka). Strong negative loadings for Asteraceae and Poaceae and weak negative loadings for *Acacia* occur on PLSR predictor axis 1 for the current glacial-interglacial. PLSR predictor axis 1 is consequently indicative for the catchment vegetation structure. Monte-Carlo modelled palaeo-sediment residence times showed strong positive loadings on response axis 1 for both the last and the current glacial-interglacial cycle (Fig. 5). A significant correlation is identified between the PLSR scores from predictor axis 1 (combined results for the last and current glacial-interglacial cycle) and catchment sediment residence times (Fig. 7A, $R^2 = 0.48$, $p < 0.005$). No significant correlation is observed between K/Ti and palaeo-sediment residence times (Fig. 7G, $R^2 = 0.19$, $p > 0.005$), but a significant negative correlation is found between K/Ti and Myrtaceae + Casuarinaceae abundance (Fig. 7H, $R^2 = 0.52$, $p < 0.005$).

The accumulation of organic carbon in the sediments of Lake Couridjah, as inferred from TOC_{acc}, resembles the variability recorded in palaeo-sediment residence times (Fig. 6). Overall higher TOC_{acc} occured in both peak interglacials (130 ka to 115 ka, and the Holocene). Somewhat higher abundances of aerophilic + epiphytic diatoms (up to 77%) were recorded between 133.5 ka and 115 ka and during the Holocene (Fig. 6), while lower abundance (less than 45%) occurred between 115 ka and 107.6 ka, when planktonic diatoms were abundant. Planktonic diatom abundance was low and variable between 133.5 ka and 115 ka, low and steady during the Last Glacial, and almost absent during the Holocene (Fig. 6).

4. Discussion

4.1 Modern catchment data

Disequilibrium of ^{238}U-^{234}U in bedrock older than 1 Ma, as recorded in our catchment data, has previously been attributed to deep weathering and fracturing. Uranium-234/^{238}U activity ratios greater than 1 can be driven by (a) the isotopic ratio of uranium rich mineral coatings and-or secondary sandstone cement, or (b) by recoil from either of these sources into the mineral grain (Reynolds et al., 2003; Dosseto and Schaller, 2016). Activity ratios < 1 detected in the rock samples collected in outcrops imply these rocks have undergone substantial weathering. Uncertainties about the initial bedrock ($^{234}U/^{238}U$) activity ratios can influence the calculated catchment sediment residence times as discussed in detail in the Supplement.

In soil pit WBRC1, higher ($^{234}U/^{238}U$) activity ratios occur at greater soil depth, close to the bedrock-weathering horizon interface, and lower ($^{234}U/^{238}U$) activity ratios occur in topsoil layer (Fig. 3). This is a common feature across SE Australia (e.g. Dosseto et al., 2008; Suresh et al., 2013), attributed to the downward migration of the bedrock to weathering horizon interface over time. It implies deeper erosion predominately mobilises detrital matter with high ($^{234}U/^{238}U$) activity ratios. Uranium-234/^{238}U activity ratios and palaeo-sediment residence times in sedimentary archives have thus been used as proxy for erosion processes and erosion depth (shallower versus deeper erosion) in settings where temporary storage in the fluvial system is considered shorter than 10,000 years (Li et al., 2018;

Rothacker et al., 2018; Francke et al., 2019). Although temporary storage of sediments >10,000 years may be expected for the alluvial fans separating the Thirlmere lakes, these features primarily consist of sand-sized material (Forbes et al., 2021). Therefore, we infer detrital matter <63 µm, targeted during uranium isotope analyses, is rapidly transported to Lake Couridjah. In the Thirlmere catchment, detrital matter with lower ($^{234}U/^{238}U$) activity ratios might be stored for extended periods in skeletal soils on the gently inclining slopes closer to the lake and on top of the ridge crests, and may be mobilised by shallower and slower erosion. Detrital matter with higher ($^{234}U/^{238}U$) activity ratios might be mobilised by somewhat deeper and faster erosion of thin skeletal soils formed on steeper slopes in vicinity of the scarps (Fig. 1). An additional contributor to erosional processes in the Thirlmere catchment may be mass wasting (rockfalls, topples) as evident in the Thirlmere catchment today, and as described elsewhere in the Sydney Basin (Tomkins et al., 2004). However, boulders and blocks mobilised during rockfalls would not contribute to the lake sediment's ($^{234}U/^{238}U$) activity ratio budget. The majority of detritus delivered to Lake Couridjah likely originates from scarps and soils below the ridge crests, with the steeper slopes being covered by thinner soils (compared to those on the ridge crests), which are also more prone to deeper erosion.

TOC and trace metal isotope geochemistry of the soil pit WBRC1 yield a strong covariance of soil depth versus time of detrital matter storage and SOC storage (Fig. 3, see Fig. S3 for correlation coefficients). The data implies shallower erosion mobilises the SOC rich topsoil layer (high TOC) and detrital matter stored in the soil and weathering horizons for an extended time (low ($^{234}U/^{238}U$) activity ratios). Deeper erosion would mobilise SOC poor horizons (low TOC) and detrital matter stored in the soil or weathering horizon for shorter time (with higher ($^{234}U/^{238}U$) activity ratios). Erosion depth would have no impact on the mobilised material's degree of chemical alteration, since there is no depth-dependent variability in K/Ti, unless saprolite is mobilised by deep erosion (Fig. 3).

4.2 The last and current glacial-interglacial cycle

4.2.1 Catchment vegetation cover and catchment erosion

Palaeo-sediment residence times are a measure of catchment erosion, which depends on catchment size and morphology, bedrock geology, chemical weathering, vegetation, and climate (Dosseto and Schaller, 2016; Francke et al., 2020a; Thollon et al., 2020). Of these factors, catchment size, morphology, and geology were effectively constant over the time interval investigated herein. Our Monte-Carlo modelling indicates chemical leaching has only limited control on calculated palaeo-sediment residence times (Supplement 1). Climate (i.e. the amount of rainfall) was also unlikely to directly control erosion, since greater humidity was previously inferred by Forbes et al. (2021) for the period between 130 ka and 115 ka (broadly equivalent to MIS5e) and the Holocene, with both periods characterised by longer palaeo-sediment residence times (Fig. 6). The strong positive loading of Myrtaceae + Casuarinaceae and strong negative loadings of Asteraceae and Poaceae on PLSR predictor axis 1, combined with the strong positive loading of palaeo-sediment residence times on PLSR response axis 1, implies aspects of vegetation can statistically predict catchment erosion and palaeo-sediment residence times (Fig. 5, 6). The representation of Myrtaceae + Casuarinaceae pollen versus Asteraceae and Poaceae probably indicates erosion processes in the Thirlmere catchment are primarily controlled by contrasting vegetation structure as represented by the relative dominance of canopy and mid-storey cover versus understorey elements represented by grasses and herbs. Myrtaceae + Casuarinaceae comprise a wide range of shrubs and trees within the Thirlmere catchment, while Asteraceae and Poaceae summarise a range of grass and herb species (Rose and Martin, 2007, Supplement; Forbes et al., 2021). The strong relationship between catchment erosion and vegetation structure is substantiated by the strong positive phase-relationship between PLSR predictor axis 1 (summarized as canopy and mid-storey cover), PLSR response axis 1 (vegetation-dependent soil erodibility), and modelled palaeo-sediment residence times (Fig. 6, 7A).

The expansion of more open- canopied and mid-storey vegetation communities, with increasing proportions of herbs and grasses, as indicated by Poaceae and Asteraceae has been used as an indicator of dry and/or colder environments in Australia (Black et al., 2006; Williams et al., 2006; Cadd et al., 2021). At Thirlmere, the expansion of Poaceae and Asteraceae along with a reduction in the projective cover by the taller strata (the canopy and mid-storey cover), particularly on the steep slopes and scarps, would result in more open vegetation cover (Fig. 8). These changes would reduce soil stability and promote the erosion of shallow soils and-or deeper erosion across the Thirlmere catchment.

A strong control of vegetation structure on erosion also consistent with *in-situ* ^{10}Be data of soils in the nearby Blue Mountains area, which suggested soil erosion is significantly lower under forests (Wilkinson et al., 2005). That study also revealed a significantly higher soil thickness under forested plateaus compared to mainly heath covered slopes. Previous studies have shown a high soil thickness, in combination with shallow sheetwash erosion under a dense vegetation canopy, translates into longer soil-detrital matter storage, and thus into longer palaeo-sediment residence times (Francke et al., 2019).

A meta-analysis of 24 Late Pleistocene to Holocene pollen records has recently shown that vegetation turnover and richness in SE Australia is mainly controlled by moisture (via tropical and westerly wind systems) and sea-level change (controlling oceanic climates, Adeleye et al., 2020). This is consistent with the expansion of herb and grass vegetation during periods of reduced regional precipitation in the Thirlmere catchment between 133.5 ka and 130 ka and between 17.8 cal ka BP and 11.6 cal ka BP (Forbes et al., 2021). This supports that moisture has negative feedback on catchment-wide erosion at Thirlmere, with drier climates not promoting slower erosion, but rather faster and deeper erosion, due to the reduction of canopy and mid-storey cover as the vegetation underwent structural change. These findings are also supported from the Murrumbidgee River palaeochannel (300 km SE of Lake Couridjah), which has been shown to have palaeo-sediment residence times an order of magnitude lower during glacial compared to interglacial periods (Dosseto et al., 2010).

Although occurring at low values only, any occurrence of *Acacia* pollen (between 0.6 and 3.5 %, pollen count generally < 6, Fig. 4) has been demonstrated to indicate the presence of these species in the mid- to upper strata of sclerophyllous vegetation communities (Dodson, 1983; Black et al., 2007; Rose and Martin, 2007) , but *Acacia* are also an abundant component of the overstorey in the direct vicinity of the lake (Supplement). *Acacia* are often indicative of drier, or frequently disturbed sclerophyll communities, but they are severely under-represented in fossil pollen data (Mariani et al., 2021). The low pollen count for *Acacia* in core LC2 complicates the interpretation of this pollen taxa in the palaeo-record. Careful evaluations of our statistical analyses indicate a strong positive (weak negative) loading of *Acacia* on predictor axis 1 during the last (current) glacial-interglacial cycle. This might suggest a difference on the control of mid- storey and/or taller canopy vegetation in the vicinity of the lake during both the last and current glacial-interglacial cycles, assuming the statistical analyses are not biased by the low pollen counts of *Acacia*.

Between 127 ka and 115 ka, Lake Couridjah's catchment vegetation increasingly changed from a canopy and mid-storey dominated vegetation structure to a grass and herb dominated, more-open vegetation structure, as inferred from decreasing Myrtaceae + Casuarinaceae and increasing Asteraceae (Fig. 4, 8). This trend is, however, not mirrored in *Acacia* and Poaceae, with both taxa appear broadly anticorrelated during this time interval. The high PLSR-derived index of canopy and mid-storey cover between 127 ka to 115 ka is therefore (statistically) mainly controlled by *Acacia* (Fig. 4), which might imply a relatively high importance of the mid-story vegetation patterns and-or upper canopy strata in the vicinity of the lake for the prediction of vegetation-dependent soil erodibility during the last interglacial cooling (Fig. 6).

High and stable palaeo-sediment residence between 127 and 123 ka, and between 120 to 115 ka imply slower and shallower erosion during periods of increased fire activity and fire-mediated vegetation disturbance (high charcoal surface area > 1 $mm^2/cm^3/yr$, high sedimentary SPAC content). Frequent disturbance by fire is probably also indicated by highly variable *Acacia*, and, to some degree Poaceae, which both respond rapidly to fire disturbance, throughout the Late Glacial and Holocene. The high variability in *Acacia* may (statistically) explain the weak negative loading on PLSR predictor axis 1 during the current glacial-interglacial, implying that *Acacia* was less significant in controlling soil erosion during the current, compared to the last, glacial-interglacial cycle (where *Acacia* shows a strong positive loading on predictor axis 1). Frequent disturbance of *Acacia* may be of particular importance during the Late Glacial, where macroscopic charcoal values are high (Fig. 6).

Late Glacial and Holocene fire activity in the Thirlmere catchment is further refined by charring intensities, as inferred from Attenuated Total Reflectance Fourier Transform Infrared spectra from the same core (Constantine et al., 2021) and increasing Late Glacial to Holocene sedimentary SPAC contents (Fig. 4, Forbes et al., 2021). Fire activity does not appear to have been related to PLSR-derived soil erodibility nor to palaeo-sediment residence times during both glacial-interglacial cycles. This is despite evidence of increased erosion and sediment delivery in post-fire rainfall and runoff events attributed to changes in soil properties (water repellency) and opening of vegetation cover (summarised in Shakesby and Doerr, 2006). The soil's water repellence might be increased, decreased, or not alerted depending on fire temperature and duration, which controls infiltration, runoff, and rainsplash detachment (Letey, 2001; Shakesby and Doerr, 2006), all of which may alter sediment supply to Lake Couridjah in post-fire environments. The lack of response in erosion to bushfire activity may be related to (i) the low sample resolution for uranium isotope analyses, (ii) the long timespan covered by samples (typically 80 to 100 years based on the sedimentation rates by Forbes et al., (2021)) providing ample background sedimentation that may overprint the fire signal, and-or (ii) by post-fire rainfall characteristics that may control weak post-fire erosion event only (Tomkins et al., 2008).

Overall short and variable palaeo-sediment residence times (< 50 kyrs) between 115 ka and 107.6 ka show very similar patters to canopy and mid-storey indicators in the pollen record (Myrtaceae + Casuarinaceae, PLSR-derived predictor axis 1), and predicted vegetation-dependent soil erodibility (Fig. 6). Short and decreasing palaeo-sediment residence times (< 50 kyrs) indicate accelerated and deeper erosion, when the vegetation structure was dominated by grasses and herbs. Relatively wet conditions, as inferred from a deeper and/or more persistent lake during the same time period (Forbes et al., 2021), could have further promoted deeper and faster catchment erosion, and thus, contributed to the shortest palaeo-sediment residence time recorded in the late last glacial-interglacial cycle. High lake levels and wetter climates imply that change in vegetation structure between 115 and 107.6 ka was probably rather controlled by temperature than by rainfall.

No pollen were preserved on top of the sedimentary hiatus between 107 ka and 17.8 cal ka BP within an oxidised silty clay unit dated between 17.8 cal ka BP and 16 cal ka BP. The long palaeo-sediment residence times (> 90 kyrs) between 17.8 cal ka BP and 16 cal ka BP similar to those observed during interglacial periods (130 ka to 115 ka, Holocene), are unlikely to be explained by changes in the vegetation cover. Colder and drier climate conditions at the end of the last Glacial (compared to interglacials) likely promoted a similar vegetation structure as observed in other glacial parts of the record (Fig. 4, Cadd et al., 2021). We speculate that higher moisture availability after 17.8 cal ka BP, as indicated by regional climates (Cadd et al., 2021) and the onset of lacustrine deposition at Lake Couridjah (Forbes et al., 2021), mobilised topsoil material or fine-grained material stored in littoral parts of the lake via increased runoff and/or wave action, material that may have previously spent an extended period stored in the catchment. This is also consistent with Forbes et al. (2021)'s interpretation that the major hiatus between 107 ka and 17.38 cal ka BP likely resulted from a combination of slow catchment erosion and aeolian deflation.

4.2.2 Soil development

The lower K/Ti in WBRC's soil samples compared to saprolite samples from the same location implies K/Ti ratios can be used as an indicator for the degree of chemical weathering and soil development in the lake's catchment. The absence of correspondence between K/Ti and palaeo-sediment residence times for the last and current glacial-interglacial cycle implies a de-coupling between soil development and catchment erosion (Fig. 7H).

Warmer and wetter climates as well as tree and forest growth is thought to represent the most important processes affecting chemical weathering (Sverdrup, 2009). A strong control of root-soil structure interactions and warmer and wetter climates on soil development in the Thirlmere catchment is also supported by the moderate strong, statistically significant negative relationship between K/Ti and Myrtaceae + Casuarinaceae (Fig. 7H).

Limited soil development between 115 and 110 ka is inferred from high K/Ti and corresponds to the transition to relatively open grass and herb vegetation cover, low root-soil structure interactions (low Myrtaceae + Casuarinaceae), and to faster and deeper erosion (low palaeo-sediment residence time, Fig. 4, 7). This indicates a negative feedback between vegetation cover, catchment erosion, and soil development during the late last interglacial cooling phase.

4.2.3 Catchment-wide carbon cycling

Overall faster erosion of thinner soils (short palaeo-sediment residence times, high PLSR vegetation-dependent soil erodibility) during colder and drier intervals (133.5 ka to 130 ka, 115 ka to 17.6 ka, Late Glacial) could have resulted in high SOC erosion rates, rapidly degrading the relatively thin OM rich topsoil layer described for the modern Thirlmere catchment (section 3.1, Fig. 8). Deeper and faster erosion could have reduced soil-microbial respiration of OM rich topsoil, since material is transported and buried in a sedimentary sink (Chappell et al., 2015). Deeper and faster erosion would also expose SOC from greater soil depths that is mainly comprised of resistant stable soil-C fractions (Chappell et al., 2015). The behaviour of stable C fraction from greater soil depths under deeper erosion is still uncertain, since this carbon pool might be more resistant to mineralisation, reducing CO_2 remobilisation into the atmosphere. However, it has also been shown deeper erosion can have 'priming effects' on carbon decomposition via the addition of more labile, 'modern' C, which can increase CO_2 remobilisation into the atmosphere (Jandl et al., 2007; Doetterl et al., 2016).

Low TOC_{acc} from the sediments of Lake Couridjah imply low net-carbon accumulation within the lake between 133.5 ka and 130 ka, between 115 ka and 107.6 ka and during Late Glacial, probably due to limited productivity in the lake, and possibly, limited soil-carbon erosion (Fig. 6, 8). Low soil-C accumulation in the lake, despite fast catchment erosion, was potentially related to overall lower productivity of the open grass and herb vegetation cover (low PLSR-vegetation canopy and mid-storey vegetation cover), since the majority of terrestrial biomass is produced by large trees in temperate Australia (Roxburgh et al., 2006). Low terrestrial biomass and mobilisation of mainly minerogenic soils by deeper erosion could have also reduced nutrient supply to the lake, which could, in combination with the inferred cold and climates (Forbes et al., 2021), restrict swamp and aquatic productivity in the lake basin. Limited amounts of aquatic to semi-aquatic (swamp) vegetation (macrophytes, sedges) are inferred from the low abundance of aerophilic + epiphytic diatom taxa (Forbes et al., 2021). Higher planktonic diatom abundances indicate higher lake levels, and the expansion of phytoplankton habitats at this time (Fig. 6). This may indicate that carbon sequestration in Lake Couridjah was more controlled by aquatic productivity of phytoplankton, particularly between 115 ka and 107.6 ka, where planktonic diatom abundance was high (Fig. 6). However, the low TOC_{acc}, despite the high planktonic diatom abundance (Fig. 6), may indicate that these high lake level phases have a reduced capacity for OM-biomass accumulation, compared to intervals with high

TOC_{acc} and high aerophilic and epiphytic diatom abundance. This is probably due to the low amount of swamp vegetation (providing the substrate for the epiphytic diatoms) being a strong contributor to the lake TOC_{acc} (Forbes et al., 2021). In summary, we infer a lower atmospheric carbon sequestration in the Thirlmere catchment between 133.5 ka and 130 ka, between 115 ka to 107.6 ka, and during the Late Glacial (compared to the wetter and warmer intervals). Climates were overall colder and drier, resulting in low catchment productivity, deeper and faster erosion, re-mineralisation of old carbon stored at greater soil depth, limited nutrient supply to the lake, and limited primary productivity by phytoplankton and aquatic to semi-aquatic plants living in the lake (Fig. 8).

Shallower and slower erosion (long palaeo-sediment residence times, low PLSR-predicted vegetation-dependent soil erodibility) could have resulted in low SOC erosion rates during warmer and wetter intervals (130 ka to 115 ka and during the Holocene). Long palaeo-sediment residence times (low PLSR-predicted vegetation-dependent soil erodibility) might promote OM oxidation, and, thus, CO_2 recycling into the atmosphere (Doetterl et al., 2016). However, a low vegetation-dependent soil erodibility, shallower and slower erosion and a more closed canopy and mid-storey cover could have also fostered longer and deeper SOC storage via bioturbation by roots (Fig. 8).

High TOC_{acc} implies high net-carbon accumulation in Lake Couridjah between 130 ka and 115 ka and during Holocene. High TOC_{acc} is attributed to higher primary productivity in the lake basin, as is observable today (Fig. 1). Significantly higher aerophilic and epiphytic diatom abundance implies the increase in TOC_{acc} was mainly related to aquatic to semi-aquatic (swamp) vegetation in the lake. Somewhat lower planktonic diatom abundance consequently implies a reduction in planktonic habitats, and lower lake levels. Aquatic and semi-aquatic productivity may be fostered by higher nutrient supply from the catchment during the overall warmer and wetter climates of these periods.

Significant contributions of terrestrial OM to the lake carbon-pool may have originated from relatively weakly decomposed topsoil SOC mobilised by shallower erosion (section 3.1, Fig. 8). Additionally, more terrestrial OM supply during warmer and wetter intervals despite reduced erosion, could probably be explained by an expansion of a canopy and mid-storey cover (Fi. 6). A canopy and mid-storey cover produces significant amounts of easily transportable, loose leaf litter in the catchment (Gordon et al., 2018), as also observed at the present day (Fig. 1), while a more closed canopy and roots prevents deeper soil erosion despite wetter conditions. In summary, we infer high atmospheric carbon sequestration both in the catchment and the wetland during the overall warmer and wetter periods between 130 ka and 115 ka and during the Holocene (Fig. 8).

4. Conclusions

Our multiproxy analyses and statistical modelling predict a strong correlation between the vegetation structure in the catchment, erosion, and soil-organic carbon storage. The results imply moisture has an indirect control on catchment-wide erosion at Thirlmere, with wetter climates promoting slower and shallower erosion due the stabilisation of catchment soils by the expansion of more closed and probably more stable vegetation structure. The development of more closed mid-storey and canopied vegetation during warm and humid periods (between 130 ka and 115 ka and during the Holocene) promoted high organic accumulation in the soils but overall reduced SOC erosion. High organic carbon accumulation rates in the lake basin during warmer and wetter periods (between 130 ka and 115 ka and during the Holocene) are attributed to high biomass productivity within the lake and the catchment. This implies an overall high potential for catchment-wide atmospheric carbon dioxide sequestration during the Holocene and between 130 ka and 115 ka (broadly equivalent to MIS5e).

Erosion was high during colder and drier periods (133.5 ka to 130 ka, 115 ka to 107.6 ka, Late Glacial), when relatively open vegetation structure promoted deeper and faster erosion of thin soils. Low aquatic and terrestrial biomass production and high SOC erosion rates during colder and drier intervals imply low catchment-wide atmospheric carbon sequestration between 133.5 ka and 130 ka, 115 ka and 107.6 ka, and during the Late Glacial.

Our research was conducted at a site with climatic, lithologic, and plant-species communities representative for SE Australia more broadly. The controls of catchment erosion in the Thirlmere catchment are furthermore supported by previous studies in the Blue Mountains (nearby Sydney) and the Murrumbidgee catchment (approximately 300 km to the southeast). This suggests our findings provide insight into the interplay of erosion and soil-carbon cycling across the broader region of SE Australia, which has previously been characterised as globally significant terrestrial carbon sink.

Declaration of competing interest

The authors declare that they have no known competing financial interests or personal relationships that could have appeared to influence the work reported in this paper.

Acknowledgment

We wish to acknowledge the long connection held by the First Nations peoples of the Dharawal people, who are the first custodians of the Woolyungah Country, which includes the Thirlmere lakes. This research was funded by the New South Wales Department of Environment and Heritage (OEH) as part of the Thirlmere Lakes Research Program to TC, AD and SM. Geochronology and laboratory analyses were supported by funding from the Australian Research Council Centres of Excellence Scheme (Project Number CE170100015). Special thanks also goes to Emily Barber, Andres Zamora, Elizabeth Swallow, Heather Haines, Brian Jones all of whom were a key part of the Thirlmere team when core LC2 was analysed.

Figure Captions

Fig. 1: A: Location of the Thirlmere lakes in SE Australia. **B:** Location of Lake Couridjah (lake 3) in Thirlmere Lakes system. White arrow indicates the location of Dry Lake **C:** Location of core LC2. Black line a' to a'' represents the vegetation and sediment transect presented in D. Black arrows and shaded area highlight the alluvial fan separating lakes Couridjah and Baraba. **D:** Topographic cross-section for the Lake Couridjah catchment (a' to a"). A to E in red indicate the major geomorphic and vegetation zones around Lake Couridjah, as shown in pictures in the lower pannel. Modified after Forbes et al. (2021).

Fig. 2: Conceptual model of detrital matter transit from source to sink. Depletion of ^{234}U starts in fine-grained detrital matter that is produced as the weathering front on the hillslopes migrates downward over time. Further lowering of the ($^{234}U/^{238}U$) activity ratio occurs in any process related to hillslope and fluvial storage and transport, and during final deposition in a

sedimentary basin. The time excluding final deposition represents the palaeo-sediment residence time. Modified after Dosseto and Schaller (2016)

Fig. 3: ($^{234}U/^{238}U$) activity ratio, $\delta^{13}C_{soil}$, $\delta^{15}N_{soil}$ isotope and elemental (TOC, TN, K/Ti) data of the WBRC soil pit from the catchment of Lake Werri Berri. The site is considered representative for the catchment of Lake Couridjah due to the homogenous bedrock lithology in the Thirlmere catchment. Carbon and nitrogen isotope data of leaf litter are from after Forbes et al. (2021). Correlation

coefficients and probabilities for correlations between isotope and elemental data are reported in Fig. S3.

Fig. 4: Terrestrial pollen, charcoal surface area, and SPAC content for the last and current glacial to interglacial cycle. Pollen, charcoal, and SPCA data were previously published by Forbes et al. (2021). Terrestrial pollen percentages were re-calculated by excluding all aquatic and semi-aquatic taxa as well as Chenopodiaceae, which occurred at very low pollen counts only.

Fig. 5: PLSR loadings for predictor (recalculated, terrestrial pollen taxa *Acacia*, Asteraceae, Poacea, Mytraceae + Casuarinaceae) and response (palaeo-sediment residence times) variables. PLSR analyses were carried out separately for the current (top panel, 17.3 cal ka BP to present day) and last (bottom panel, 133,5 ka to 1107.6 ka) glacial to interglacial cycle.

Fig. 6: Palaeo-sediment residence times, $\delta^{13}C_{lake}$, $\delta^{15}N_{lake}$, K/Ti, TOC_{acc}, diatom, and PLSR-derived mid-upper story vegetation density and vegetation-depended soil erodibility versus age. The age model was previously published by Forbes et al. (2021). Dashed vertical lines mark major climate boundaries of the penultimate glacial, early last interglacial (broadly equivalent to MIS5e), late last interglacial, Late Glacial, and Holocene. Note reverse scale for K/Ti. Total diatom abundance is balanced by species classified as “others” if they could not be classified as of Aerophilic, Epiphytic or Planktonic (see Forbes et al., 2021 for more details).

Fig. 7: Scatter plots, correlation coefficients and probabilities for palaeo-sediment residence times, Mytraceae + Casuarinaceae, and K/Ti ratios of core LC2. The data are presented for the entire core

LC2, i.e. statistical analyses presented in Fig. 7 were not carried out separately for the current and last glacial to interglacial cycle as conducted for PLSR analyses.

Fig. 8: Conceptual model of vegetation change, catchment erosion, SOC-mobilisation, and lake-productivity in the Thirlmere catchment during warmer and wetter (peak-last interglacial, Holocene) and colder and drier (penultimate glacial, late-last interglacial and Late Glacial) periods. Letters A to D mark different landscapes in the Thirlmere catchment and are the same as for Fig. 1D.

Bibliography

Adeleye, M.A. et al., 2020. Long-term drivers of vegetation turnover in Southern Hemisphere temperate ecosystems. Global Ecology and Biogeography.

Black, M.P., Mooney, S.D., Haberle, S.G., 2007. The fire, human and climate nexus in the Sydney Basin, eastern Australia. The Holocene, 17(4): 469-480.

Black, M.P., Mooney, S.D., Martin, H.A., 2006. A >43,000-year vegetation and fire history from Lake Baraba, New South Wales, Australia. Quaternary Science Reviews, 25(21-22): 3003-3016.

Bureau of Meteorology, 2021. Australian climate data from 1889 to yesterday.

Cadd, H. et al., 2021. A continental perspective on the timing of environmental change during the last glacial stage in Australia. Quaternary Research, 102: 5-23.

Chappell, A., Baldock, J., Sanderman, J., 2015. The global significance of omitting soil erosion from soil organic carbon cycling schemes. Nature Climate Change, 6(2): 187-191.

Constantine, M. et al., 2021. Using charcoal, ATR FTIR and chemometrics to model the intensity of pyrolysis: Exploratory steps towards characterising fire events. Science of The Total Environment, 783.

DePaolo, D.J., Maher, K., Christensen, J.N., McManus, J., 2006. Sediment transport time measured with U-series isotopes: Results from ODP North Atlantic drift site 984. Earth and Planetary Science Letters, 248(1-2): 394-410.

Dodson, J.R., 1983. Modern pollen rain in southeastern new South Wales, Australia. Review of Palaeobotany and Palynology, 38(3): 249-268.

Doetterl, S. et al., 2016. Erosion, deposition and soil carbon: A review of process-level controls, experimental tools and models to address C cycling in dynamic landscapes. Earth-Science Reviews, 154: 102-122.

Dosseto, A., Hesse, P.P., Maher, K., Fryirs, K., Turner, S., 2010. Climatic and vegetation control on sediment dynamics during the last glacial cycle. Geology, 38(5): 395-398.

Dosseto, A., Schaller, M., 2016. The erosion response to Quaternary climate change quantified using uranium isotopes and in situ-produced cosmogenic nuclides. Earth-Science Reviews, 155: 60-81.

Dosseto, A., Turner, S.P., Chappell, J., 2008. The evolution of weathering profiles through time: New insights from uranium-series isotopes. Earth and Planetary Science Letters, 274(3–4): 359-371.

Forbes, M. et al., 2021. Comparing interglacials in eastern Australia: A multi-proxy investigation of a new sedimentary record. Quaternary Science Reviews, 252.

Francke, A., Carney, S., Wilcox, P., Dosseto, A., 2018. Sample preparation for determination of comminution ages in lacustrine and marine sediments. Chemical Geology, 479: 123-135.

Francke, A. et al., 2019. Sediment residence time reveals Holocene shift from climatic to vegetation control on catchment erosion in the Balkans. Global and Planetary Change, 177: 186-200.

Francke, A. et al., 2020a. Geochemical methods to infer landscape response to Quaternary climate change and land use in depositional archives: A review. Earth-Science Reviews, 207: 103218.

Francke, A., Dosseto, A., Just, J., Wagner, B., Jones, B.G., 2020b. Assessment of the controls on (234U/238U) activity ratios recorded in detrital lacustrine sediments. Chemical Geology, 550: 119698.

Gordon, C.E., Bendall, E.R., Stares, M.G., Collins, L., Bradstock, R.A., 2018. Aboveground carbon sequestration in dry temperate forests varies with climate not fire regime. Glob Chang Biol, 24(9): 4280-4292.

Haverd, V. et al., 2013. The Australian terrestrial carbon budget. Biogeosciences, 10(2): 851-869.

Haverd, V., Smith, B., Trudinger, C., 2016. Dryland vegetation response to wet episode, not inherent shift in sensitivity to rainfall, behind Australia's role in 2011 global carbon sink anomaly. Glob Chang Biol, 22(7): 2315-6.

Horsfall, L., Jelinek, A., Timms, B.V., 1988. The influence of recreation, mainly power boating, on the ecology of the Thirlmere Lakes, N.S.W., Australia. SIL Proceedings, 1922-2010, 23(1): 580-587.

Kaplan, J.O., Krumhardt, K.M., Zimmermann, N., 2009. The prehistoric and preindustrial deforestation of Europe. Quaternary Science Reviews, 28(27): 3016-3034.

Klein Goldewijk, K., Beusen, A., Doelman, J., Stehfest, E., 2017. Anthropogenic land use estimates for the Holocene – HYDE 3.2. Earth System Science Data, 9(2): 927-953.

Letey, J., 2001. Causes and consequences of fire-induced soil water repellency. Hydrological Processes, 15(15): 2867-2875.

Li, F. et al., 2020. Towards quantification of Holocene anthropogenic land-cover change in temperate China: A review in the light of pollen-based REVEALS reconstructions of regional plant cover. Earth-Science Reviews, 203: 103119.

Li, L. et al., 2018. Weathering dynamics reflected by the response of riverine uranium isotope disequilibrium to changes in denudation rate. Earth and Planetary Science Letters, 500: 136-144.

Lugato, E. et al., 2018. Soil erosion is unlikely to drive a future carbon sink in Europe. Science Advances, 4(11): eaau3523.

Luo, Y. et al., 2016. Toward more realistic projections of soil carbon dynamics by Earth system models. Global Biogeochemical Cycles, 30(1): 40-56.

Mariani, M. et al., 2021. Disruption of cultural burning promotes shrub encroachment and unprecedented wildfires. Frontiers in Ecology and the Environment.

Martin, A.N. et al., 2019. Sediment residence times in catchments draining to the Gulf of Carpentaria, northern Australia, inferred by uranium comminution dating. Geochimica et Cosmochimica Acta, 244: 264-291.

Poulter, B. et al., 2014. Contribution of semi-arid ecosystems to interannual variability of the global carbon cycle. Nature, 509(7502): 600-3.

Reynolds, B.C., Wasserburg, G.J., Baskaran, M., 2003. The transport of U- and Th-series nuclides in sandy confined aquifers. Geochimica et Cosmochimica Acta, 67(11): 1955-1972.

Rose, S., Martin, H.A., 2007. The Vegetation History of the Holocene at Dry Lake, Thirlmere, New South Wales. Proceedings of the Linnean Society of New South Wales, 128: 15-55.

Rothacker, L. et al., 2018. Impact of climate change and human activity on soil landscapes over the past 12,300 years. Scientific Reports, 8(1): 247.

Roxburgh, S.H., Wood, S.W., Mackey, B.G., Woldendorp, G., Gibbons, P., 2006. Assessing the carbon sequestration potential of managed forests: a case study from temperate Australia. Journal of Applied Ecology, 43(6): 1149-1159.

Shakesby, R., Doerr, S., 2006. Wildfire as a hydrological and geomorphological agent. Earth-Science Reviews, 74(3-4): 269-307.

Short, M.A. et al., 2020. Two centuries of water-level records at Lake George, NSW. Australian Journal of Earth Sciences: 1-20.

Sugita, S., 2007a. Theory of quantitative reconstruction of vegetation I: pollen from large sites REVEALS regional vegetation composition. The Holocene, 17(2): 229-241.

Sugita, S., 2007b. Theory of quantitative reconstruction of vegetation II: all you need is LOVE. The Holocene, 17(2): 243-257.

Suresh, P.O., Dosseto, A., Hesse, P.P., Handley, H.K., 2013. Soil formation rates determined from uranium-series isotope disequilibria in soil profiles from the southeastern Australian highlands. Earth and Planetary Science Letters, 379: 26-37.

Sverdrup, H., 2009. Chemical weathering of soil minerals and the role of biological processes. Fungal Biology Reviews, 23(4): 94-100.

Thollon, M. et al., 2020. The distribution of (234U/238U) activity ratios in river sediments. Geochimica et Cosmochimica Acta, 290: 216-234.

Timms, B.V., 1992. Lake Geomorphology. Gleneagles Publishing, Adelaide.

Tomkins, K.M. et al., 2008. Postwildfire hydrological response in an El Niño–Southern Oscillation–dominated environment. Journal of Geophysical Research, 113(F2).

Tomkins, K.M. et al., 2004. Mass movement events in the south-west Sydney basin during the Holocene Regolith. In: I.C., R. (Ed.), Regolith 2004. CRC LEME, pp. 365-369.

Trondman, A.K. et al., 2015. Pollen-based quantitative reconstructions of Holocene regional vegetation cover (plant-functional types and land-cover types) in Europe suitable for climate modelling. Glob Chang Biol, 21(2): 676-97.

van Dijk, A.I.J.M. et al., 2013. The Millennium Drought in southeast Australia (2001-2009): Natural and human causes and implications for water resources, ecosystems, economy, and society. Water Resources Research, 49(2): 1040-1057.

Wilkinson, M.T. et al., 2005. Soil production in heath and forest, Blue Mountains, Australia: influence of lithology and palaeoclimate. Earth Surface Processes and Landforms, 30(8): 923-934.

Williams, N.J., Harle, K.J., Gale, S.J., Heijnis, H., 2006. The vegetation history of the last glacial–interglacial cycle in eastern New South Wales, Australia. Journal of Quaternary Science, 21(7): 735-750.

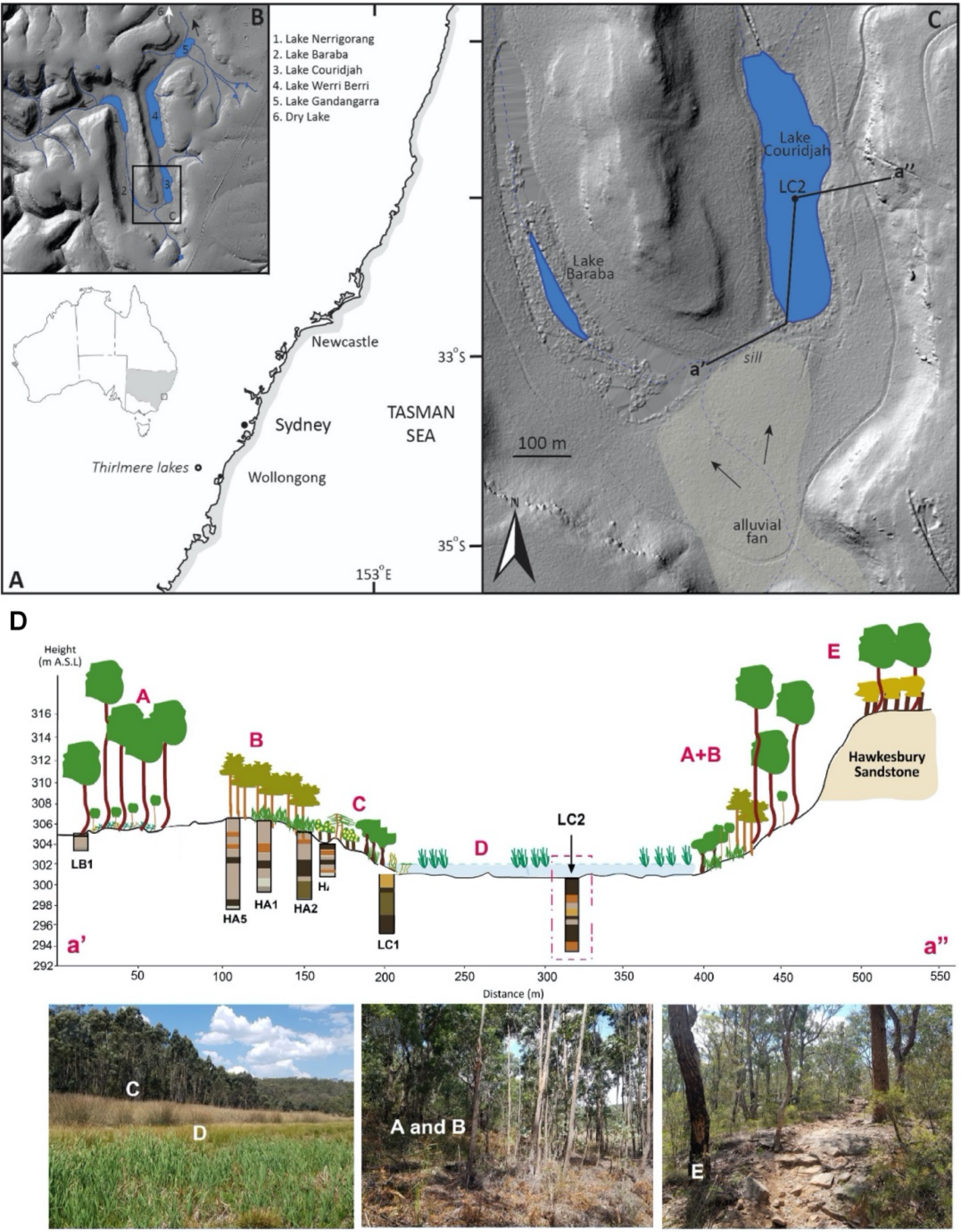

B
1. Lake Nerrigorang
2. Lake Baraba
3. Lake Couridjah
4. Lake Werri Berri
5. Lake Gandangarra
6. Dry Lake
C
Lake Couridjah
LC2
a''
Lake Baraba
a'
sill
100 m
N
alluvial fan
Newcastle
33°S
Sydney
TASMAN SEA
Thirlmere lakes
Wollongong
35°S
153°E
A
D
Height (m A.S.L)
316
314
312
310
308
306
304
302
300
298
296
294
292
A
B
C
D
A+B
E
Hawkesbury Sandstone
LC2
LB1
HA5
HA1
HA2
LC1
a'
a''
50
100
150
200
250
300
350
400
450
500
550
Distance (m)
C
D
A and B
E

Fig. 1

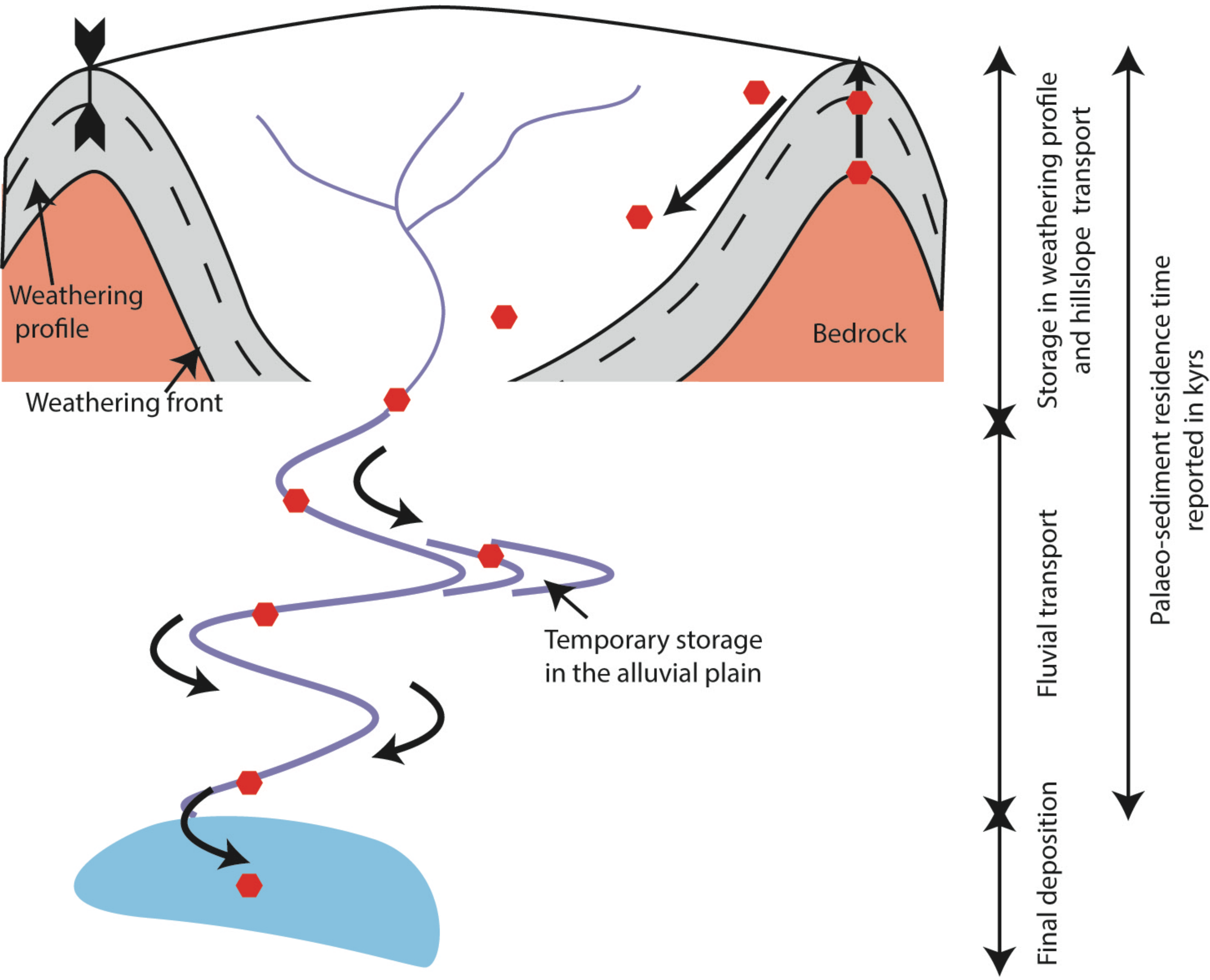
Weathering profile
Weathering front
Bedrock
Temporary storage in the alluvial plain
Storage in weathering profile and hillslope transport
Fluvial transport
Final deposition
Palaeo-sediment residence time reported in kyrs

Fig. 2

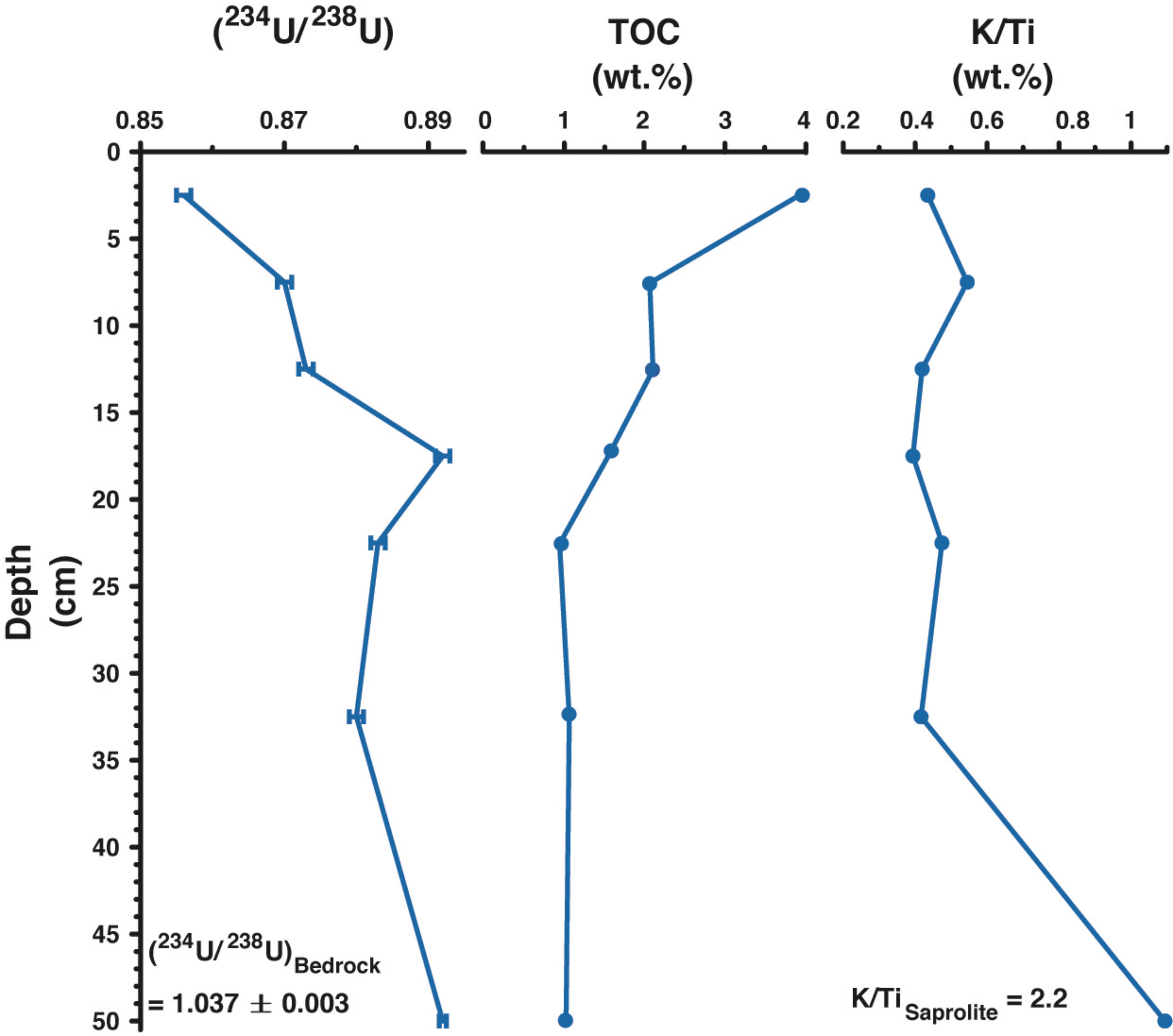

$(^{234}U/^{238}U)$
TOC
(wt.%)
K/Ti
(wt.%)
0.85
0.87
0.89
0
1
2
3
4
0.2
0.4
0.6
0.8
1
0
5
10
15
20
25
30
35
40
45
50
Depth
(cm)
$(^{234}U/^{238}U)_{Bedrock}$
$= 1.037 \pm 0.003$
$K/Ti_{Saprolite} = 2.2$

Fig. 3

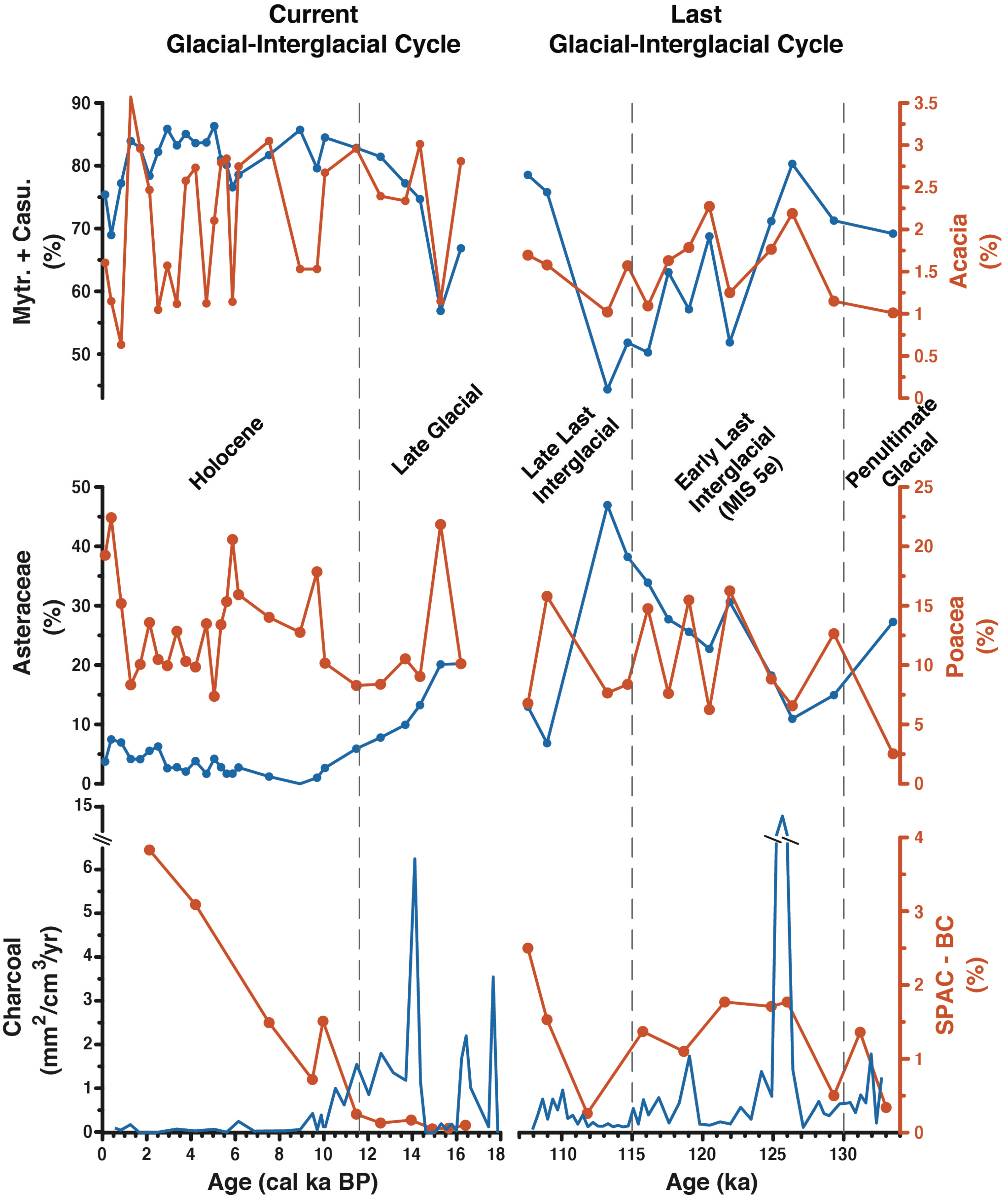
Current
Glacial-Interglacial Cycle
Last
Glacial-Interglacial Cycle
Mytr. + Casu. (%)
Acacia (%)
Holocene
Late Glacial
Late Last Interglacial
Early Last Interglacial (MIS 5e)
Penultimate Glacial
Asteraceae (%)
Poacea (%)
Charcoal (mm²/cm³/yr)
SPAC - BC (%)
Age (cal ka BP)
Age (ka)

Fig. 4

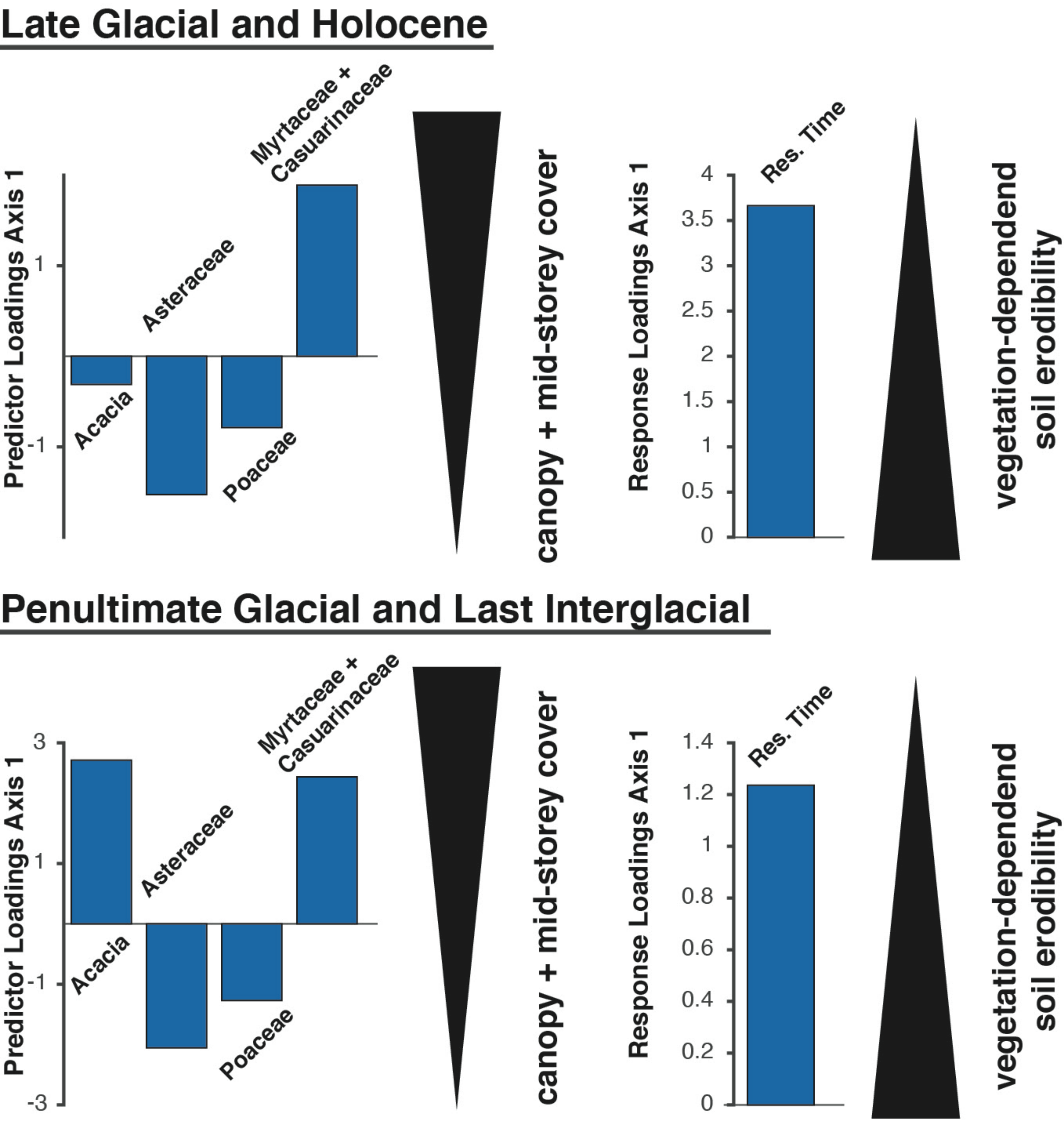

Late Glacial and Holocene
Predictor Loadings Axis 1
1
-1
Acacia
Asteraceae
Poaceae
Myrtaceae +
Casuarinaceae
canopy + mid-storey cover
Response Loadings Axis 1
4
3.5
3
2.5
2
1.5
1
0.5
0
Res. Time
vegetation-dependend
soil erodibility
Penultimate Glacial and Last Interglacial
Predictor Loadings Axis 1
3
1
-1
-3
Acacia
Asteraceae
Poaceae
Myrtaceae +
Casuarinaceae
canopy + mid-storey cover
Response Loadings Axis 1
1.4
1.2
1
0.8
0.6
0.4
0.2
0
Res. Time
vegetation-dependend
soil erodibility

Fig. 5

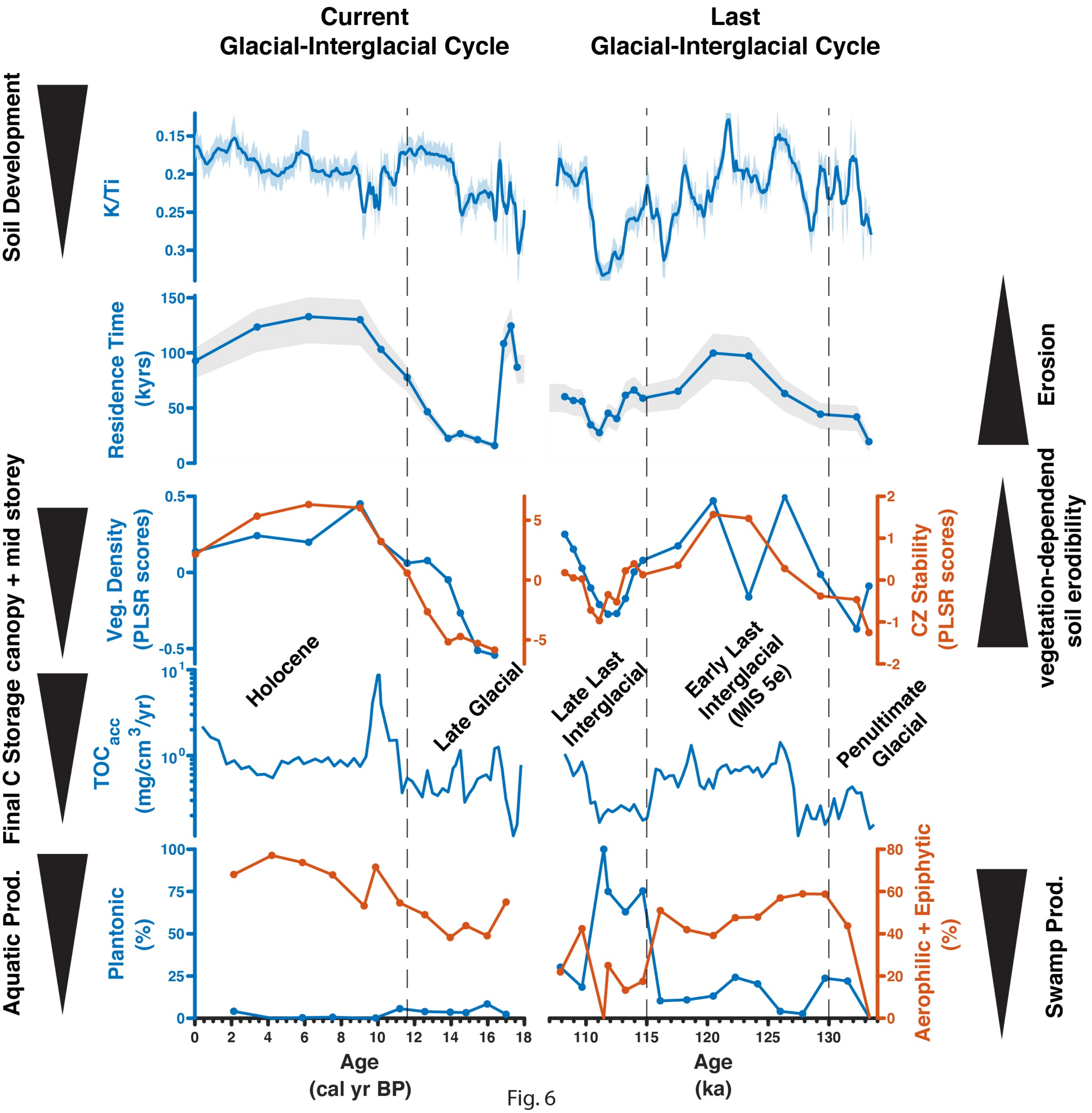

Current
Glacial-Interglacial Cycle
Last
Glacial-Interglacial Cycle
Soil Development
K/Ti
Residence Time (kyrs)
Erosion
Final C Storage canopy + mid storey
Veg. Density (PLSR scores)
CZ Stability (PLSR scores)
vegetation-dependend soil erodibility
TOC_{acc} ($mg/cm^3/yr$)
Holocene
Late Glacial
Late Last Interglacial
Early Last Interglacial (MIS 5e)
Penultimate Glacial
Aquatic Prod.
Plantonic (%)
Aerophilic + Epiphytic (%)
Swamp Prod.
Age (cal yr BP)
Age (ka)

Fig. 6

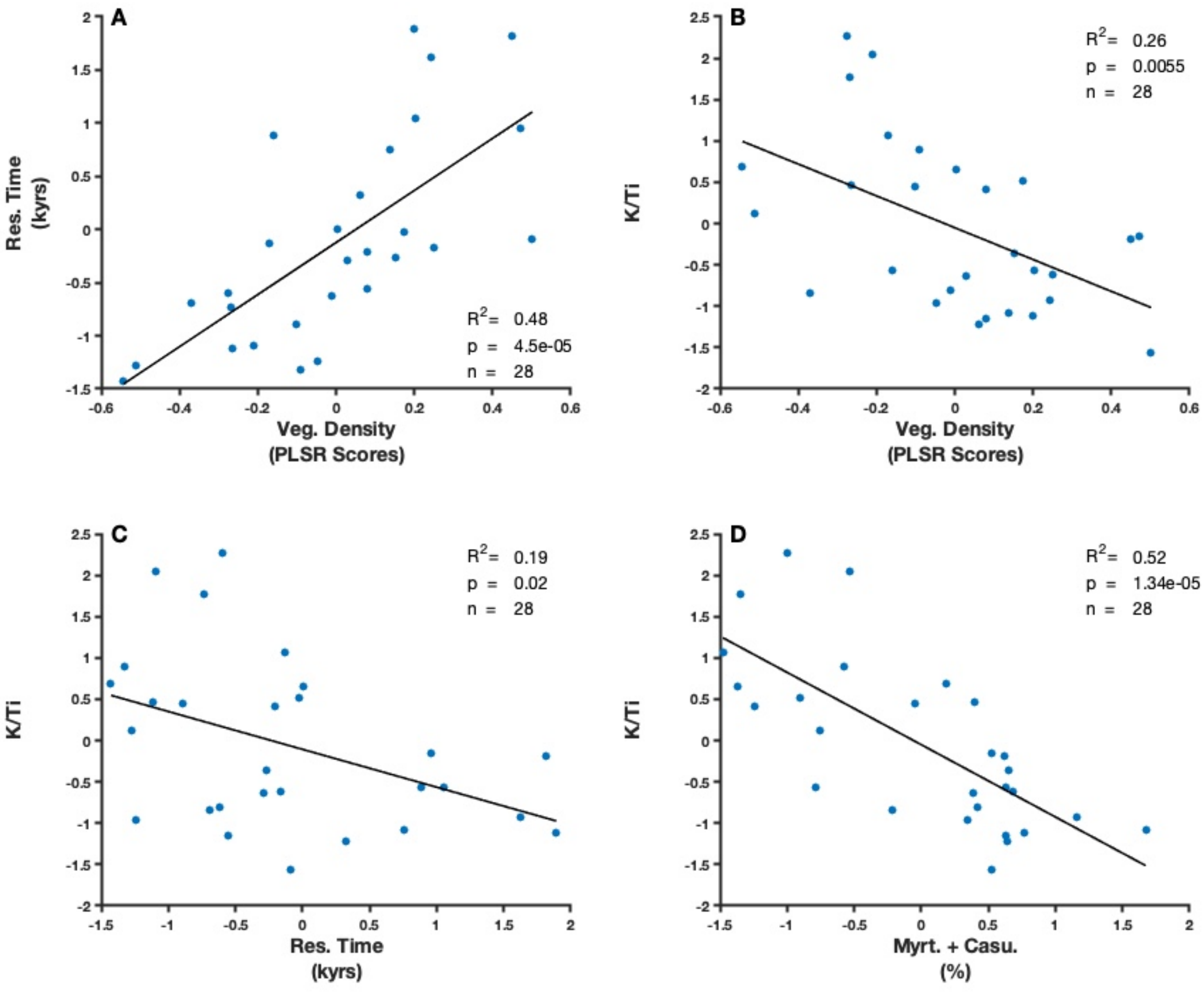
A
Res. Time
(kyrs)
Veg. Density
(PLSR Scores)
R2= 0.48
p = 4.5e-05
n = 28
B
K/Ti
Veg. Density
(PLSR Scores)
R2= 0.26
p = 0.0055
n = 28
C
K/Ti
Res. Time
(kyrs)
R2= 0.19
p = 0.02
n = 28
D
K/Ti
Myrt. + Casu.
(%)
R2= 0.52
p = 1.34e-05
n = 28

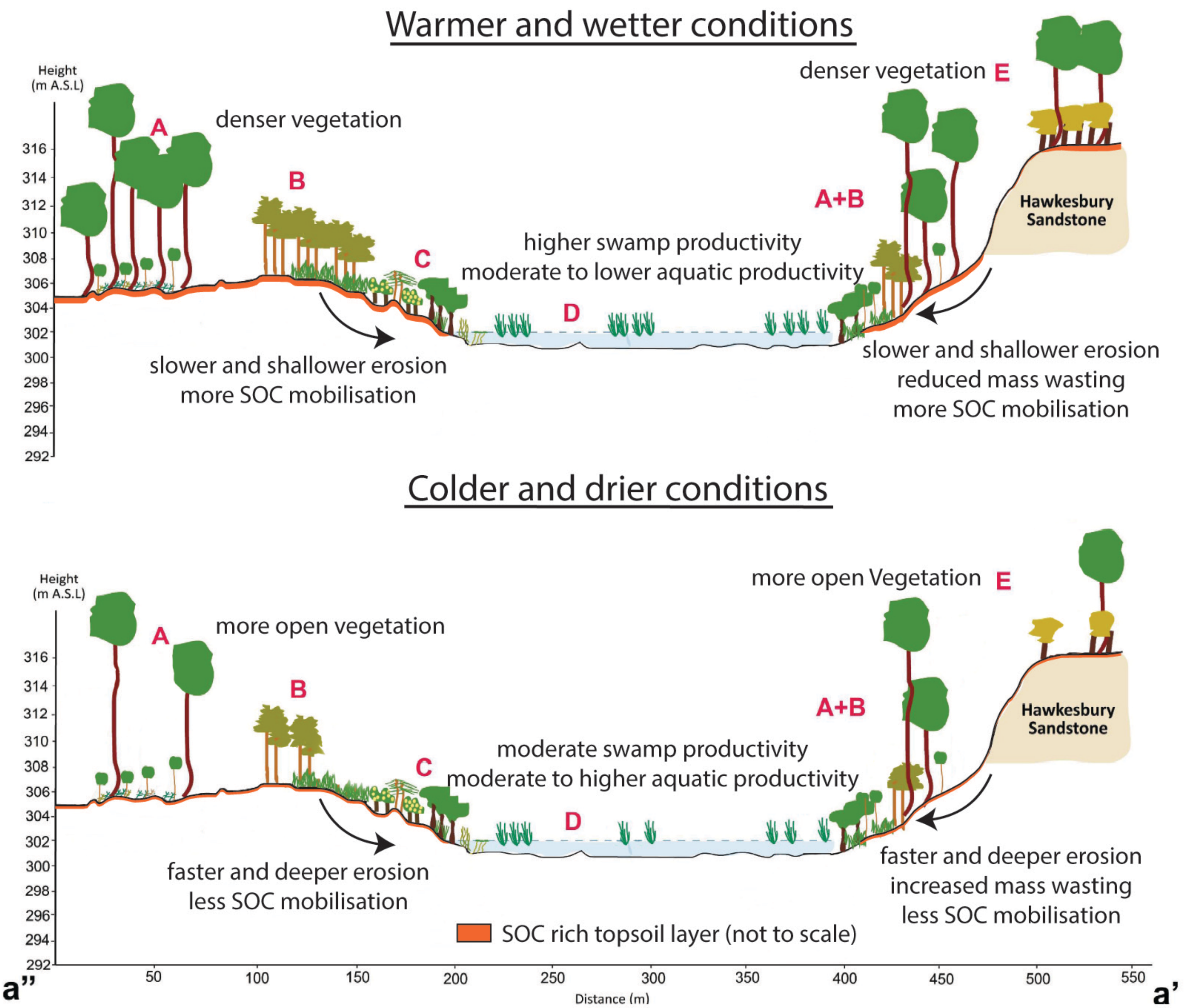

Warmer and wetter conditions
Height (m A.S.L)
316
314
312
310
308
306
304
302
300
298
296
294
292
A
denser vegetation
B
C
higher swamp productivity
moderate to lower aquatic productivity
D
denser vegetation E
A+B
Hawkesbury Sandstone
slower and shallower erosion
more SOC mobilisation
slower and shallower erosion
reduced mass wasting
more SOC mobilisation
Colder and drier conditions
Height (m A.S.L)
A
more open vegetation
B
C
moderate swamp productivity
moderate to higher aquatic productivity
D
more open Vegetation E
A+B
Hawkesbury Sandstone
faster and deeper erosion
less SOC mobilisation
faster and deeper erosion
increased mass wasting
less SOC mobilisation
SOC rich topsoil layer (not to scale)
a''
50
100
150
200
250
300
350
400
450
500
550
a'
Distance (m)

Supplement

1. Regional settings

The detailed survey of the contemporary vegetation patterns in the direct vicinity of Lake Couridjah by Forbes et al. (2021) imply that open mixed sclerophyll forest (mainly Myrtaceae incl. *Eucalyptus piperita, E. nitens* and *E. deanei*, *Corymbia gummifera and C. eximia*) cover the top of the ridge crests and the alluvial fans to the north and south of Lake Couridjah, as well as gullies and slopes along the eastern and western flank of the lake (Areas A, B, and E in Fig. 1). Open dry sclerophyll midstory in the same areas mainly composes of Casuarinaceae (*Allocasuarina torulosa*), Proteaceae (*Xylomelum pyriforme, Persoonia linearis, Banksia serrata*), and Apiaceae (*Platysace linearfolia*). Fabaceae (*Acacia longifolia, Acacia linearfolia*) and Dennstaedtiaceae (*Histiopteris incisa*) are most prominent midstory vegetation in closer proximity to the lake but can also be found on the alluvial fans and top of the ridge crests. The lake margin and lakebed of Lake Couridjah are covered by Cyperaceae (*Lepironia articulata*, *Lepidosperma longitudinale*) during wetter intervals, and by herbs and other species including *Gonocarpus micranthus* (Haloragaceae), *Cyperus difformis* and *Juncus planifolius* (Cyperaceae), *Philydrum lanuginosum* (Philydraceae) and invasive species like *Paspalum dilatatum* (Poaceae) during dry periods. Vegetation growing in the lake (during wetter periods) and on the lakebed (during dryer periods) promote the formation of a peat/swamp environment at Lake Couridjah today.

2. Methods

2.1 Major element and stable isotope geochemistry (WBRC1 soil pit)

Total organic carbon (TOC) analyses was determined after combustion at 1150°C using a vario MICRO cube element analyser (Elementar) as released CO_2 and N_2 at the University of Wollongong (Wollongong, Australia). Conventional XRF analyses (for Ti and K content) were first combusted at 960°C to determine loss on ignition (LOI), mixed with flux and then fused at 1150° in Pt-Au (platinum-gold) crucibles. Element concentration analysis was conducted on pressed powder pellets and analysed at the University of Wollongong (Wollongong, Australia) using a desktop Spectro XEPOS energy dispersive spectrometer.

2.2 Uranium isotope analyses

A Neptune Plus (ThermoScientific) Multi-Collector Inductive Coupled Plasma Mass Spectrometer (MC-ICP MS) equipped with a PFA-self aspirating nebulizer and an ESI Apex IR desolvator for introduction of samples and standards was used for uranium isotope analyses. After passing through a jet sample and x skimmer cones, ^{235}U and ^{238}U were collected on Faraday cups, while a secondary electron multiplier (SEM) equipped with a retarding potential quadrupole (RPQ) was used to collect ^{234}U and ^{236}U. Correction for mass bias and SEM/Faraday cup yield and precision was assessed by analysing a synthetic standard NBL U010 before and after each sample. Isotopic ratios are reported as ($^{234}U/^{238}U$) activity ratios. Standard deviation from a NBL U005A synthetic standard at the start and end of each sequence was consistently better than 0.5% (Table 1). Total procedure blanks showed that blanks contributed <0.2% to the analysed isotopic ratios. Accuracy and precision were assessed by analysing USGS BCR-2 and QLO-01a reference materials and in total six replicates from the core and soil pit samples (Table 1). Reference material, primary and secondary standards was evaluated against expected accuracy from the literature (Sims et al., 2008). U concentrations were determined by isotope dilution for all double $^{236}U/^{229}Th$ spiked samples, and by means of quadrupole ICP-MS analyses at the University of Wollongong for all other samples.

2.2 Surface area and surface properties

Surface area and surface properties were analysed by gas absorption analysis on a Quantachrome Autosorb iQ. Samples were first degassed for 7.5 h (5 °C/min to 80 °C, soak time 30 min, followed by 1 °C/min to 100 °C, soak time 60 min, followed by 5 °C/min to 200 °C, soak time 300 min). Best fit of the Multi-point BET equation was used to determine the specific surface area. Micropores not relevant for loss by ^{234}Th recoil were determined and subtracted by using the t-method of Halsey (1948).

2.3 Palaeo-sediment residence time calculations

Palaeo-sediment residences times were calculated based on a modified equation to that of DePaolo et al. (2006). The new equation of Francke et al. (2020) is based on those of Dosseto and Schaller (2016) and allows accounting for realistic values of pre- and post-depositional leaching of ^{234}U and limited loss of ^{234}Th after final deposition, which can overprint the actual recoil loss of ^{234}U since comminution by ^{234}Th recoil. The modified equation reads as follows:

$$t_{res} = \frac{-1}{\lambda_{234}+\left(\frac{w_{234pre}}{w_{238pre}}-1\right)*w_{238pre}} \ln\left[\frac{[A_{meas}-(1-f_{post})]e^{-\lambda_{234}t_{dep}}+(1-f_{post})-\left(\frac{(1-f_{pre})*\lambda_{234}}{\lambda_{234}+\left(\frac{w_{234pre}}{w_{238pre}}-1\right)*w_{238pre}}\right)}{A_0-\left(\frac{(1-f_{pre})*\lambda_{234}}{\lambda_{234}+\left(\frac{w_{234pre}}{w_{238pre}}-1\right)*w_{238pre}}\right)}\right] \quad (1)$$

where f_{pre} and f_{post} are the recoil loss factors before and after final deposition, A_{meas} is the measured ($^{234}U/^{238}U$) activity ratio (unitless), A_0 the initial ($^{234}U/^{238}U$) activity ratio, i.e. prior to comminution (unitless), λ_{234} the ^{234}U decay constant (in yr^{-1}), and t_{dep} the deposition age (in years), as derived from the age-depth model. The recoil loss factors f_{pre} and f_{post} are a function of the grain surface area and are defined as follows (Kigoshi, 1971; Maher et al., 2006):

$$f = \frac{1}{4} LS\rho \quad (2)$$

with L is the recoil length of ^{234}Th (in m), ρ the density of the sediment (in g/m^3), and S the surface area of the sediment (m^2/g). We use a Monte Carlo simulation (10,000 simulations) with input variables presented in Table S3. Considerations about site-specific input variables (A_0, f_{pre}, f_{post}, S, w_{238pre}, $w_{238post}$) are provided below, all other variables are taken from the literature (Table S2).

Uranium-234/^{238}U activity ratios of bedrock sampled in the Thirlmere catchment that deviate from expected secular equilibrium are attributed to subareal weathering (for outcrop samples) and to mineral coatings, secondary sandstone cement and/or deep weathering fractures (cf. main text). We relax the assumption of an initial bedrock activity ratio of 1 in our palaeo-sediment residence time calculations by randomly choosing A_0 between 1 and 1.03 in our Monte-Carlo simulations, with A_0 = 1.03 as inferred from ($^{234}U/^{238}U$) activity ratio inferred from Hawkesbury sandstone at 21 m bedrock depth.

Preferential leaching of ^{234}U before and/or after deposition can yield lower ($^{234}U/^{238}U$) activity ratios that are not related to recoil induced loss of ^{234}Th. Maher et al. (2004) inferred that the amount of preferential leaching of ^{234}U can be approximate by $w_{238} \approx 0.1 Age^{-1}$. We herein follow a conservative approach suggested by Francke et al. (2020) by using lowest estimated palaeo-sediment residence times (to maximise w_{238}) to infer the detrital matter's age, and we use the equation of Maher et al. (2004) to calculate w_{238pre} *and* $w_{238post}$ (Table S2). The impact of different scenarios of pre- and post-depositional preferential leaching is presented in Fig. S2.

Loss of ^{234}Th by recoil might be reduced after final deposition in densely compacted depositional archives due to (a) grain to grain recoil, (b) secondary matter (such as organic matter, carbonates) or pore fluid to grain recoil and/or (c) adsorption to mineral surfaces or coatings (Dosseto and Schaller, 2016; Priestley et al., 2018). A previous study has demonstrated that considerations about reduced loss of ^{234}Th by recoil after final deposition has no major impact on modelled palaeo-sediment residence in depositional sediments younger than the Late Glacial (Francke et al., 2019). This is also supported by different scenarios for tested for f_{post} in this study, where Late Glacial to Holocene sediments how palaeo-sediment residences within error of each other in depended of chosen values for f_{post} (Fig. S2). Not accounting for reduced loss of ^{234}Th by recoil after final deposition however leads to unrealistically low and negative palaeo-sediment residences times in the sediments of the last glacial/interglacial complex. A precise estimate of recoil loss of ^{234}Th after final deposition remains challenging and could probably only obtained by detailed mass-balancing between recorded (^{234}U/^{238}U) activity ratios of detrital matter, secondary matter (such as organic matter or secondary minerals), and pore waters. Different considerations for f_{post} have however no direct impact on recorded palaeo-sediment residence time variability and amplitude across the sediments of the last glacial/interglacial complex (Fig. S2). Interpretations about the catchment's response to environmental forcing for the time interval between 139 and 103 ka are therefore not affected. Uncertainties about f_{post} however hamper a direct comparison of absolute palaeo-sediment residence times for the last versus the current glacial/interglacial complex, a comparison which is therefore not attempt in this study. We find that f_{post} = 0.25* f_{pre} yields reasonable palaeo-sediment residence times for the last glacial/interglacial complex.

There is a moderately strong negative relationship between estimated external surface area and OM content (R^2 = 0.5, not shown), and samples from *peat* or *organic silty clay* generally yield zero micropore areas (Fig. S1). This is probably explained by organic matter (OM) coating of detrital grains since oxidation of OM rich sediments is frequently incomplete (Mikutta et al., 2005). Incomplete removal of OM during applied sequential leaching has however no impact on recorded (^{234}U/^{238}U) activity ratios, since uranium is thought to be comprehensively leached from remaining OM (Francke et al., 2020). Previous studies have however show that the detrital matter's micro to mesopores surface area can be reduced by occluding OM (Kaiser and Guggenberger, 2003). We therefore conclude that samples with zero micropore area are significantly affect by clogging of micro- and mesopores. We consequently relax the assumption of very low external surface area in OM rich deposits and choose S between 28 m^2/g and 66 m^2/g for palaeo-sediment time calculations, i.e. within the range of values recorded in silty clay and/or clayey sand.

Tables

Table 1: Rock standards and blanks analysed along trace metal samples.

	U (ppm*/ pg**)	**U 2σ** (ppm*/ pg**)	**($^{234}U/^{238}U$)**	**($^{234}U/^{238}U$) 2σ**	**Comment**
BCR-2	1.75	0.01	0.997	0.005	Neptune
BCR-2	1.01	0.001	0.998	0.002	Neptune
BCR-2	0.96	0.002	0.998	0.003	Neptune
BCR-2	1.26	0.10			Q-ICAP
QLO-01a	1.42	0.05			Q-ICAP
QLO-01a	1.61	0.01	0.999	0.004	Neptune
QLO-01a	1.08	0.002	1.001	0.003	Neptune
QLO-01a	0.83	0.001	1.003	0.003	Neptune
Blank	196.69	1.92	1.004	0.039	Neptune
Blank	144.5	1.4	1.002	0.022	Neptune
Blank	242.9	1.3	0.902	0.016	Neptune
Blank	176.0	0.6	1.033	0.020	Neptune
Blank	7.7	26.7			Q-ICAP
Blank	21.0	15.3			Q-ICAP
LC2-40 cm+	0.95	0.10	0.773	0.003	
LC2-180cm+	1.19	0.003	0.811	0.003	
LC2-302cm+	1.46	0.01	0.706	0.005	
LC2-410 cm+	2.02	0.01	0.811	0.005	
LC2-410 cm+	1.83	0.01	0.819	0.004	
WBRC1-22.5cm+	1.90	0.34	0.886	0.002	

*for rock standards and replicates, **for blanks, +replicates

Table 2: Input parameter for palaeo-sediment residence time modelling as shown in the main text.

Parameter	Value	Source
A_{meas}	Analysed	measured
A_0	1-1.03	Between secular equilibrium and Hawkesbury Sandstone at 21m depth

f_{pre}	Calculated	Eq. (2)
f_{post}	Calculated	f_{pre}* 0.25
t_{dep}	Calculated	Chronology of Forbes et al. (2021)
λ_{234}	2.826×10^{-6} yr^{-1}	
L	30 nm	Dosseto and Schaller (2016)
ρ	2.6×10^{-6} g/cm^3	
S	28 m^2/g to 66 m^2/g	measured
w_{234pre}/w_{238pre}	1.2 ± 0.2	(Dosseto et al., 2006; Dosseto et al., 2014)
w_{238pre}	1.11×10^{-6} yr^{-1}	Calculated after Maher et al., 2004
$w_{234post}/w_{238post}$	1.2 ± 0.2	Dosseto et al. (2006, 2014)
$w_{238post}$	6.67×10^{-7} yr^{-1}	Calculated after Maher et al. (2004)

Figure Captions

Fig. S1: Lithology and radiocarbon and luminescence data of core LC2. All data presented were previously published by Forbes et al. (2021).

Fig. S2: Palaeo-sediment residence times modelled using 10,000 MonteCarlo Simulations with difference leaching parameters w_{238} and w_{234}/w_{238}. The experiments were carried out to test the impact of preferential leaching of ^{234}U on estimated palaeo-sediment residence times. See supplementary text for more details.

Bibliography

DePaolo, D.J., Maher, K., Christensen, J.N., McManus, J., 2006. Sediment transport time measured with U-series isotopes: Results from ODP North Atlantic drift site 984. Earth and Planetary Science Letters, 248(1-2): 394-410.

Dosseto, A., Bourdon, B., Gaillardet, J., Mauricebourgoin, L., Allegre, C., 2006. Weathering and transport of sediments in the Bolivian Andes: Time constraints from uranium-series isotopes. Earth and Planetary Science Letters, 248(3-4): 759-771.

Dosseto, A., Buss, H.L., Chabaux, F., 2014. Age and weathering rate of sediments in small catchments: The role of hillslope erosion. Geochimica et Cosmochimica Acta, 132: 238-258.

Dosseto, A., Schaller, M., 2016. The erosion response to Quaternary climate change quantified using uranium isotopes and in situ-produced cosmogenic nuclides. Earth-Science Reviews, 155: 60-81.

Forbes, M. et al., 2021. Comparing interglacials in eastern Australia: A multi-proxy investigation of a new sedimentary record. Quaternary Science Reviews, 252.

Francke, A., Dosseto, A., Just, J., Wagner, B., Jones, B.G., 2020. Assessment of the controls on (234U/238U) activity ratios recorded in detrital lacustrine sediments. Chemical Geology: 119698.

Francke, A. et al., 2019. Sediment residence time reveals Holocene shift from climatic to vegetation control on catchment erosion in the Balkans. Global and Planetary Change, 177: 186-200.

Halsey, G., 1948. Physical Adsorption on Non-Uniform Surfaces. The Journal of Chemical Physics, 16(10): 931-937.

Kaiser, K., Guggenberger, G., 2003. Mineral surfaces and soil organic matter. European Journal of Soil Science, 54(2): 219-236.

Kigoshi, K., 1971. Alpha-recoil Thorium-234: Dissolution into water and the uranium-234/uranium-238 disequilibrium in nature. Science, 173(3991): 47.

Maher, K., DePaolo, D.J., Lin, J.C.-F., 2004. Rates of silicate dissolution in deep-sea sediment: In situ measurement using 234U/238U of pore fluids. Geochimica et Cosmochimica Acta, 68(22): 4629-4648.

Maher, K., Steefel, C.I., DePaolo, D.J., Viani, B.E., 2006. The mineral dissolution rate conundrum: Insights from reactive transport modeling of U isotopes and pore fluid chemistry in marine sediments. Geochimica et Cosmochimica Acta, 70(2): 337-363.

Mikutta, R., Kleber, M., Kaiser, K., Jahn, R., 2005. Review: organic matter removal from soils using hydrogen peroxide, sodium hypochlorite, and disodium peroxodisulfate. Soil Science Society of America Journal, 69(1): 120-135.

Priestley, S.C. et al., 2018. Use of U-isotopes in exploring groundwater flow and inter-aquifer leakage in the south-western margin of the Great Artesian Basin and Arckaringa Basin, central Australia. Applied Geochemistry, 98: 331-344.

Sims, K.W.W. et al., 2008. An Inter-Laboratory Assessment of the Thorium Isotopic Composition of Synthetic and Rock Reference Materials. Geostandards and Geoanalytical Research, 32(1): 65-91.

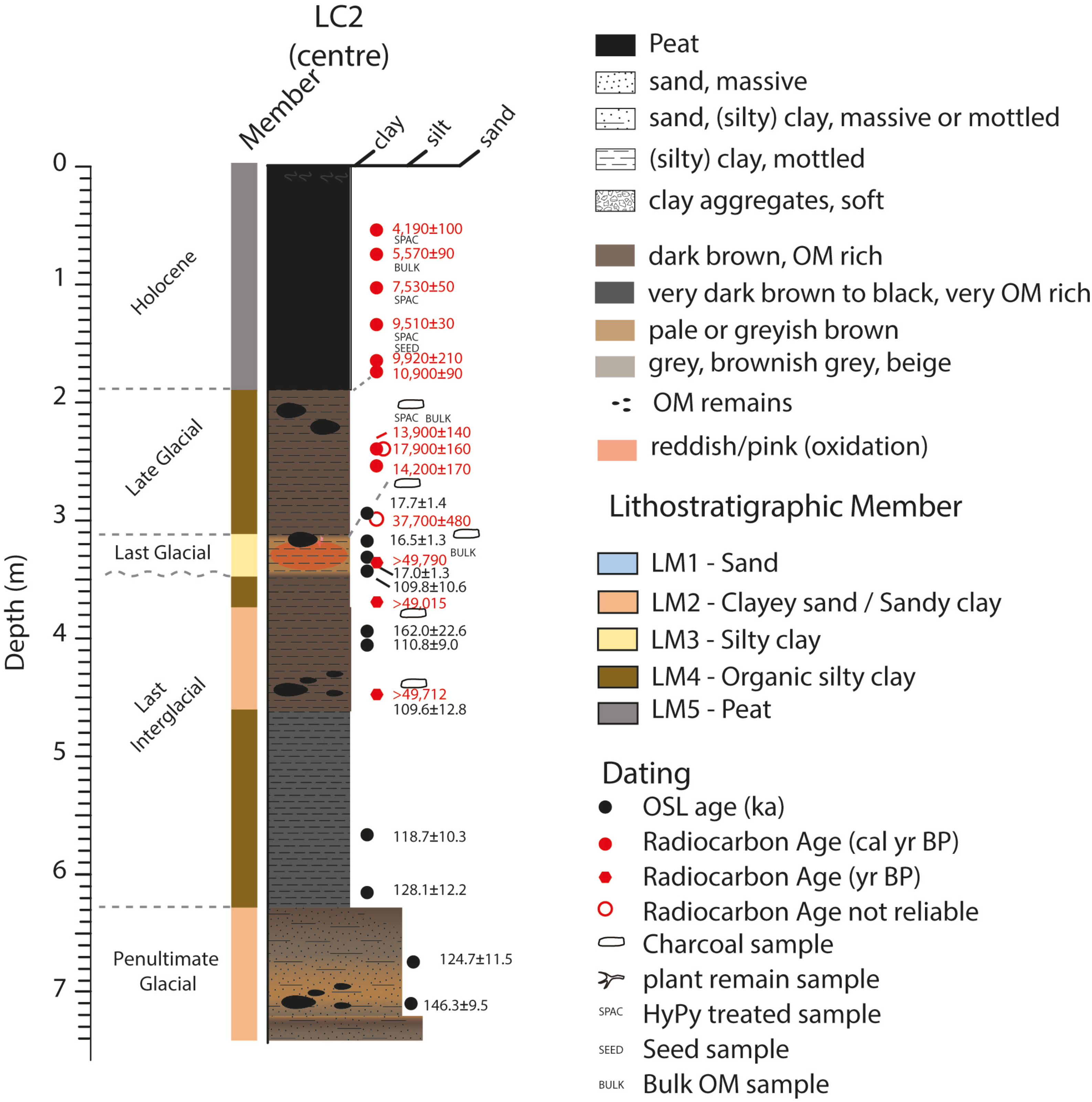

LC2
(centre)
Member
clay
silt
sand
Depth (m)
0
1
2
3
4
5
6
7
Holocene
Late Glacial
Last Glacial
Last Interglacial
Penultimate Glacial
4,190±100
SPAC
5,570±90
BULK
7,530±50
SPAC
9,510±30
SPAC
SEED
9,920±210
10,900±90
SPAC BULK
13,900±140
17,900±160
14,200±170
17.7±1.4
37,700±480
16.5±1.3
BULK
>49,790
17.0±1.3
109.8±10.6
>49,015
162.0±22.6
110.8±9.0
>49,712
109.6±12.8
118.7±10.3
128.1±12.2
124.7±11.5
146.3±9.5
Peat
sand, massive
sand, (silty) clay, massive or mottled
(silty) clay, mottled
clay aggregates, soft
dark brown, OM rich
very dark brown to black, very OM rich
pale or greyish brown
grey, brownish grey, beige
OM remains
reddish/pink (oxidation)
Lithostratigraphic Member
LM1 - Sand
LM2 - Clayey sand / Sandy clay
LM3 - Silty clay
LM4 - Organic silty clay
LM5 - Peat
Dating
OSL age (ka)
Radiocarbon Age (cal yr BP)
Radiocarbon Age (yr BP)
Radiocarbon Age not reliable
Charcoal sample
plant remain sample
SPAC HyPy treated sample
SEED Seed sample
BULK Bulk OM sample

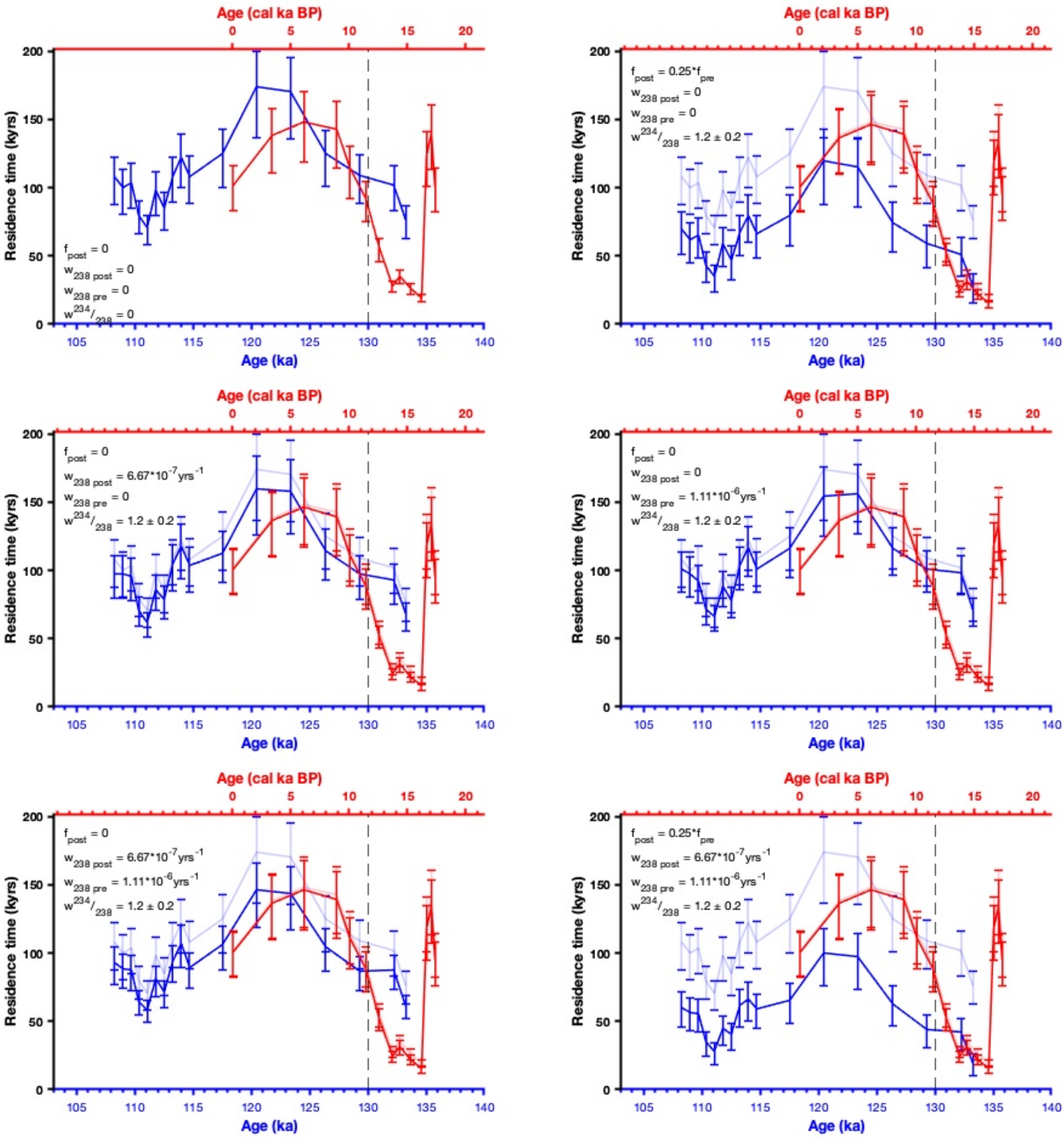

Age (cal ka BP)
Residence time (kyrs)
Age (ka)
f_post = 0
w_238 post = 0
w_238 pre = 0
w^234/_238 = 0
Age (cal ka BP)
Residence time (kyrs)
Age (ka)
f_post = 0.25*f_pre
w_238 post = 0
w_238 pre = 0
w^234/_238 = 1.2 ± 0.2
Age (cal ka BP)
Residence time (kyrs)
Age (ka)
f_post = 0
w_238 post = 6.67*10^-7yrs^-1
w_238 pre = 0
w^234/_238 = 1.2 ± 0.2
Age (cal ka BP)
Residence time (kyrs)
Age (ka)
f_post = 0
w_238 post = 0
w_238 pre = 1.11*10^-6yrs^-1
w^234/_238 = 1.2 ± 0.2
Age (cal ka BP)
Residence time (kyrs)
Age (ka)
f_post = 0
w_238 post = 6.67*10^-7yrs^-1
w_238 pre = 1.11*10^-6yrs^-1
w^234/_238 = 1.2 ± 0.2
Age (cal ka BP)
Residence time (kyrs)
Age (ka)
f_post = 0.25*f_pre
w_238 post = 6.67*10^-7yrs^-1
w_238 pre = 1.11*10^-6yrs^-1
w^234/_238 = 1.2 ± 0.2